Estimating Canopy Height in Tropical Forests: Integrating Airborne LiDAR and Multi-Spectral Optical Data with Machine Learning

Brianna Pickstone
Student Number: 720008520
Orcid ID: https://orcid.org/0009-0007-6688-2949
Supervisors: Dr Andy Cunliffe, Dr Hugh Graham
University of Exeter in partnership with Permian Global

Abstract: Accurate assessment and mapping of biomass in tropical forests is essential for understanding the contribution of forests to the global carbon budget, climate dynamics and informing environmental policies. Canopy height is an important predictor of above ground biomass. To increase the accuracy of canopy height models, characteristics of fine resolution remote sensing technology has been widely adopted. Spaceborne and airborne light detection and ranging (LiDAR) based methods can provide accurate horizontal and vertical information at high resolution. However, these methods are expensive to deploy and airborne LiDAR does not offer global coverage. To address this, freely available Synthetic Aperture Radar (SAR) and optical data from various satellite missions such as Landsat, Sentinel-1 (S1), and Sentinel-2 (S2) have been used to generate canopy height models. Data derived from PlanetScope compliments S2 data and has an increase in spatial resolution and temporal coverage compared to S2. This has provided a potential of generating more accurate canopy height models. However, few studies have compared the performance of Sentinel-2 data with PlanetScope data to estimate canopy height derived from LiDAR, especially in intricate tropical forest structures. The main aim of this study was to enhance canopy height predictions in the Katingan Mentaya Project, Central Kalimantan by comparing the performance of three machine learning algorithms (Multiple Linear Regression, Random Forest, and Convolutional Neural Networks) when using PlanetScope data and Sentinel-2 data. In all cases the random forest model and the convolutional neural network outperformed multiple linear regression. However, this study has revealed that RF may be more appropriate for predicting canopy height over a CNN due to the ease in model building, computational time, and feature selection. This study revealed the data source most appropriate for predicting canopy height was the S2 data at 10 m resolution, which model took a total of 34.23 minutes and yielded an R^2 of 0.68, with an RMSE of 3.52 m and an MAE of 2.63 m. Although the combined dataset of PlanetScope and Sentinel-2 had a slightly higher R^2 of 0.69, PlanetScope data is not always freely available, and therefore using Sentinel-2 allows for more accessible and consistent data sourcing. Overall, this study presents a helpful step towards improving the monitoring of tropical forests, as it contributes to the generation of accurate canopy height models, which are crucial for understanding forest structure, carbon storage estimation, and effective land management.

Keywords: LiDAR, PlanetScope, Planet Labs, Sentinel-2, Canopy Height, Multiple Linear Regression, Random Forest, Convolutional Neural Network

---

1. Introduction

Tropical forests are a biodiversity hotspot (Reid, 1998), accommodating approximately two-thirds of the planet's terrestrial biodiversity (Gardner et al., 2009). They are valued globally due to the multitude of terrestrial ecosystem services they provide to nature and societal wellbeing (Kacic and Kuenzer, 2022; Manning et al., 2018; Pan et al., 2011; Sharma et al., 2019), including carbon sequestration, water regulation, soil fertility, erosion control, and ecotourism (Brandon, 2014; Ditt et al., 2010; Millennium Ecosystem Assessment, 2005; Naime et al., 2020). However, the existence of tropical forests face challenges due to climate change, alteration in land, and degradation caused by logging, understory fires and fragmentation (Longo et al., 2020; Mills et al., 2023). The remaining and recovering forests are important in the global carbon budget, as they play a critical role in the carbon cycle, serving as a terrestrial carbon sink and absorbing excess carbon from the atmosphere (Leuschner et al., 2013; Mills et al., 2023; Mitchard, 2018; Pan et al., 2011). Due to this, conservation of the Earth's forests has become a priority on the worldwide political agenda and are included within the United Nation's plan of REDD+ (Reduce Emissions from Deforestation and forest Degradation, and forest conservation, sustainable management of forests, and enhancement of forest carbon stocks) (Fayad et al., 2021; Lang et al., 2022a). The REDD+ program was introduced at the United Nations Framework Convention on Climate Change (UNFCCC) Conference of Parties in 2005, playing an integral role in the sustainable management of forests and enhancement of forest carbon stocks (Corbera and Schroeder, 2011).

Permian Global is mission-led business that are pioneering new approaches within the protection and recovery of tropical forests, and are one of the major players in the voluntary carbon market (Permian Global, 2023a). Their mission is to protect and see the recovery of rainforests, making their projects align with REDD+ (Permian Global, 2023a). However, REDD+ programs have received criticism, where there has been doubt of whether the reported reductions in carbon dioxide emissions truly reflect a decrease in overall emissions (Bayrak and Marafa, 2016). Therefore, for these large-scale tropical forest restoration and protection projects to be successful, accurate and viable methods for estimating carbon components within tropical forests, including above ground biomass is essential (Ding et al., 2021; Fayad et al., 2021; Lang et al., 2022b; Pan et al., 2011; Takagi et al., 2015). This becomes particularly important when such endeavours are funded through the sale of verified carbon credits. However, the exact quantity of carbon stored in above ground biomass remains uncertain due to inconsistent measurement methodologies, and the current utilisation of Earth-observation techniques are not optimised for precise quantification of carbon density (Kellner et al., 2023; Mitchard, 2018). Inaccurate assessments of above ground biomass can have detrimental effects on conservation endeavours and lead to misallocation of carbon credits (Lang et al., 2022b; Strassburg et al., 2020). Therefore, to enhance the precision of carbon credits, developing more accurate methods for measuring and monitoring above-ground biomass is essential.

One method of estimating above ground biomass, is the generation of canopy height models (CHM), which is the vertical distance between the ground and the top of the tree canopy (Wang and Glenn, 2008). Canopy height is an important predictor of above ground biomass and carbon stock (Cunliffe et al., 2022, 2020; Dubayah et al., 2010; Jucker et al., 2017; Lang et al., 2022b; Li et al., 2020; McIntire et al., 2022; Nandy et al., 2021). Canopy height can be measured through different methods ranging from manual on-ground assessment through to using different remote sensing techniques (Csillik et al., 2020; Valluvan et al., 2023). However, the manual measurement of canopy height can be a difficult, time consuming and a labour-intensive task, and in some cases it is not feasible due to complex terrain structures of tropical forests (Constantino et al., 2018; Torres de Almeida et al., 2022; Valluvan et al., 2023). Therefore, the use of fine resolution remote sensing technologies has been adopted at local and global scales, allowing for the opportunity to increase the accuracy and predictions of canopy height (Dubayah et al., 2010; Fayad et al., 2021; Gupta and Sharma, 2023; Lin et al., 2020; Torres de Almeida et al., 2022). These predictive capabilities offer significant potential for aiding forest management choices, improving resource distribution and enhancing initiatives for biodiversity conservation.

Of particular interest are the LiDAR (Light Detection and Ranging) systems, which have the ability to precisely map the vertical structure of forests. LiDAR systems work by emitting laser pulses and calculating the difference between the sent signal and the reflected response (Dubayah et al., 2010; Fayad et al., 2021; Lang et al., 2022a; Lim et al., 2003; Torres de Almeida et al., 2022). LiDAR technology is adept at capturing the arrangement of forest elements as it can penetrate the canopy at varying depths (García et al., 2018). However, Airborne Laser Scanning (ALS) LiDAR usually only allows for small regional projects due to the financial costs involved (N. Lang et al., 2019). Further to this, it is limited by persistent cloud cover, especially in the tropics (N. Lang et al., 2019; Pourshamsi et al., 2021). To aid precise and cost-effective assessments of canopy height, satellite remote sensing data has been integrated with LiDAR data, allowing for canopy height models to be upscaled beyond areas of LiDAR coverage (Ota et al., 2014; Shimizu et al., 2020; Wilkes et al., 2015). Various optical and synthetical aperture radar (SAR) satellite data has been adopted in predicting canopy height including Landsat, Sentinel-1 (S1) and Sentinel-2 (S2) (Ahmed et al., 2015; Anderson et al., 2004; Gupta and Sharma, 2023; Hudak et al., 2002; N. Lang et al., 2019; Li et al., 2020; Liu et al., 2019; Shah et al., 2020; Torres de Almeida et al., 2022; Zhang et al., 2019). However, Li et al. (2020) compared the performance of data from these missions and found S1 and S2 demonstrated higher performance compared to Landsat-8, due to the addition of other variables such as the backscattering coefficients from Sentinel-1 and the red-edge variables in Sentinel-2. Further to this, Torres de Almeida et al. (2022) compared the potential of S1 and S2 for modelling canopy height, and found that the S2 outperformed the S1, with S1 having the higher error rates and overall a lower R^2 value, potentially due to S1's C-band that has low capacity to penetrate the canopy of forests that are structurally complex (Pourshamsi et al., 2021).

S2 allows for comprehensive monitoring of forest ecosystem dynamics and functionality worldwide, and has been found to facilitate the estimation of canopy height (Ghosh et al., 2020; N. Lang et al., 2019; Li et al., 2020; Liu et al., 2019; Torres de Almeida et al., 2022; Xi et al., 2022). The European Space Agency's Copernicus Sentinel-2 mission comprises a constellation of two polar-orbiting satellites (European Space Agency, 2023a). S2 is equipped with passive optical sensors with a spatiotemporal resolution of 10 m ~ 20 m and a revisit cycle of five days (European Space Agency, 2023a; Li et al., 2020). The success of the upscaling process is determined by the presence of a strong correlation between vegetation attributes, such as height obtained from LiDAR data and the co-variables derived from satellite data, such as spectral reflectance and vegetation indices (Li et al., 2020). The combination of LiDAR data with optical remote sensing images has been suggested as one of the most advantageous methods for obtaining canopy height (Ahmed et al., 2015; Li et al., 2020; Zhang et al., 2019).

Recent advancements in optical data missions, such as CubeSats, provide unique spatial and temporal observations due to the large constellations of satellites. PlanetScope, provided by Planet is one of the largest CubeSat constellations obtaining images that are approximately 3 meters per pixel resolution (Planet Labs, 2023a) and has been used in the upscaling process of CHM derived from LiDAR, due to its historical availability and frequent observation (Shimizu et al., 2020). Norway's International Climate and Forest Initiative (NICFI) has provided access to fine resolution optical satellite data (NICFI, 2020; Planet Labs, 2023b). The NICFI was launched in 2008 by the Norwegian Government, and has pledged up to 3 billion Norwegian Krone (NOK) a year to help save the world's tropical forests (NICFI, 2020). As part of this initiative includes Planet Labs users to access their high-resolution, analysis-ready mosaics of the world's tropics, with the aim to *"reduce and reverse the loss of tropics forests, combat climate change, conserve biodiversity and facilitate sustainable development for non-commercial users"* (Planet Labs, 2023b). This includes access to PlanetScope data, which is an excellent source for vegetation monitoring and compliments Senintel-2 (S2) data, with an increase in spatial resolution and temporal coverage (Sentinel-Hub, 2023a).

Although previous studies have investigated the utilisation of remote sensing data to predict canopy height, the majority of studies have incorporated satellites such as Landsat-8, Sentinel-1 (S1) and Sentinel-2 (S2) (Ahmed et al., 2015; Gupta and Sharma, 2023; N. Lang et al., 2019; Li et al., 2020; Liu et al., 2019; Shah et al., 2020; Torres de Almeida et al., 2022; Zhang et al., 2019). However, there have been few studies investigating the utilisation of PlanetScope data for upscaling LiDAR data and predicting canopy height, especially in tropical forest regions. Further to this, investigation into how PlanetScope compares to Sentinel-2 are lacking. Shimizu (2020) has investigated how PlanetScope data compares to Landsat 8 and Sentinel-2, for estimating airborne LiDAR derived canopy height,

however, this was completed in a temperate forest in Japan and did not explore whether the combination of these different data sources could improve canopy height prediction.

Through the use of machine learning algorithms, robust and accurate predictive models of canopy height can be generated (Brodrick et al., 2019; Csillik et al., 2020; Torres de Almeida et al., 2022). The success of the upscaling LiDAR data is determined by the presence of a strong correlation between vegetation attributes, such as height obtained from LiDAR data and the co-variables derived from satellite data, such as spectral reflectance and vegetation indices (Li et al., 2020). Parametric models, such as multiple linear regression (MLR) are commonly employed to establish forest attributes and remote sensing predictors (Dube et al., 2015; Kulawardhana et al., 2014; Sheridan et al., 2014; Torres de Almeida et al., 2022; Zhang et al., 2019). MLR is also commonly used as a good baseline model for comparison to more complex machine learning techniques. However, non-parametric machine learning models have gained popularity in recent years due to their ability of capturing complex non-linear relationships (Zhang et al., 2019). This includes Random Forest (RF) (Csillik et al., 2020; Dube et al., 2015; Fayad et al., 2021; Gupta and Sharma, 2023; Pourshamsi et al., 2021; Torres de Almeida et al., 2022; Zhang et al., 2019), Support Vector Machines (SVM) (Gupta and Sharma, 2023; Pourshamsi et al., 2021; Zhang et al., 2019), Gradient Boosting (GB) (Csillik et al., 2020; Dube et al., 2015), and Deep Learning methods such as Convolutional Neural Networks (CNN) (ElGharbawi et al., 2023; Fayad et al., 2021; Lang et al., 2022b). Further to this, non-parametric machine learning models are able to handle issues related to dimensionality when fitting models with a large number of predictors (Hudak et al., 2008; Zhang et al., 2019). The Random Forest machine learning ensemble algorithm has gained increasing attention within the remote sensing field, over the last two decades (Breiman, 2001) due to its simplicity, ability to handle complex relationship and robustness to outliers in training data, and its perceived interpretability due to feature importance scores (Wilkes et al., 2015). However, RF lacks the ability to utilise the spatial association of neighbouring pixels within raster data (Shah et al., 2020). One method that overcomes these shortcomings is the CNN, which has the ability to utilise the spatial association of neighbouring pixels in the modelling process (Shah et al., 2020). Despite this, only a limited number of studies have employed non-parametric machine learning algorithms to predict canopy height from optical remote sensing data, calibrated with LiDAR derived data.

In this study, the performance of multi-spectral optical data from PlanetScope to predict canopy height in a tropical forest was compared to Sentinel-2 data using three different machine learning algorithms (Multiple Linear Regression, Random Forest, and Convolutional Neural Network). Each model was then used to predict canopy height, and their ability to estimate canopy height derived from LiDAR data was evaluated. This study also included a comprehensive examination of the three machine learning algorithms, going beyond assessing the predictive accuracy. It also focused on how

well the algorithms can be reproduced and reliably deployed in real-world applications by taking into consideration the computational time of each algorithm.

2. Methodology

2.1 Study Area

The focal study area was Permian Global's Katingan Mentaya Project, located in the southern region of Central Kalimantan, Indonesia (latitude -2.579, longitude 113.146) (Figure 1). The project entered into partnership with Permian Global in December 2013 to ensure long-term financial stability (IETA, 2018). The project encompasses 1,498 km^2 of tropical forest and peatland, generating an average of 7.5 million triple gold certified carbon credits annually, making it the world's largest forest-based avoided emission project (Katingan Mentaya Project, 2023; Permian Global, 2023b). The area has a relatively flat terrain with an elevation range from 1.97 m to 9.78 m above sea level, with an average slope of 2.09º. Only a small area of the study site will be used to predict canopy height (Figure 1). The conservation project supports faunal species including five critically endangered species, eight endangered species and 31 vulnerable species, including the Borneo Orangutan, Southern Bornean Gibbon and the Proboscis Monkey (Permian Global, 2023b). The Katingan contains at least six High Conservation Value (HCV) floral species including the *Shorea balangeran* and *Shorea teysmanniana* (Katingan Mentaya Project, 2023).

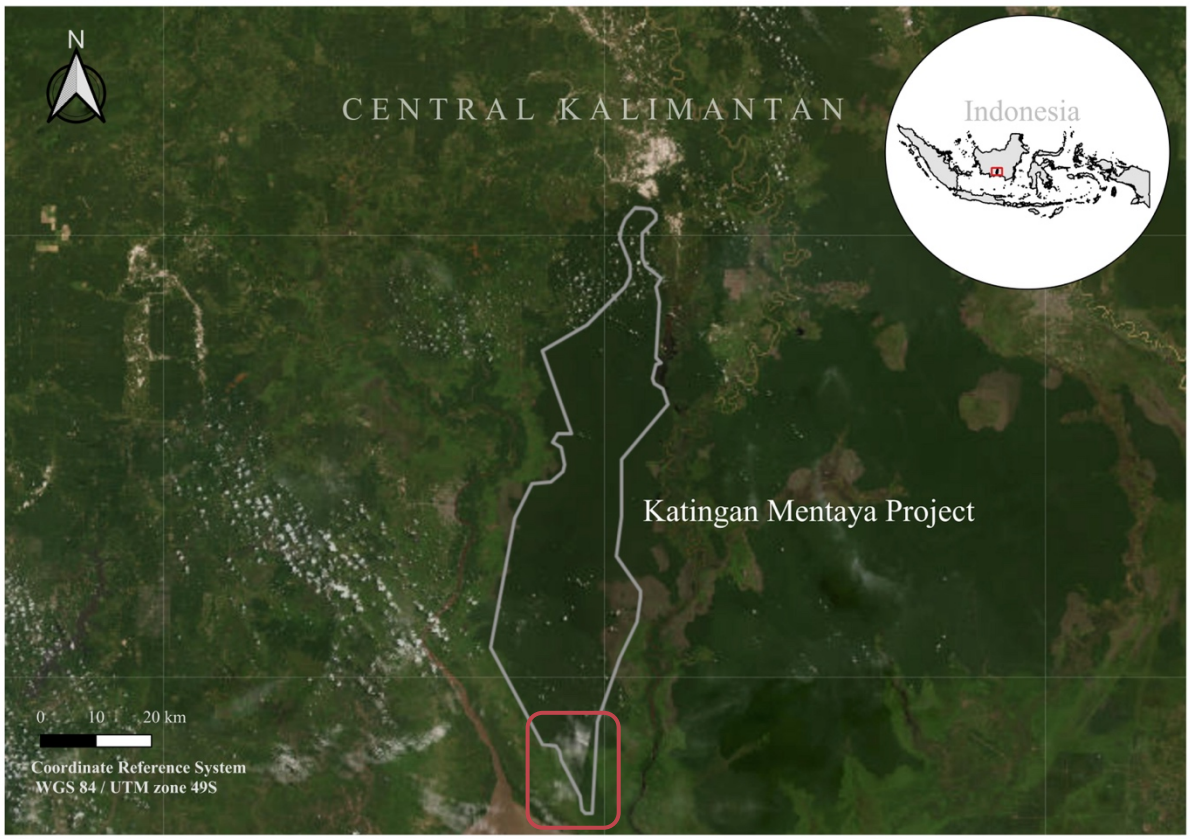

Figure 1. Geographical location of the study area, Katingan Mentaya Project, in Central Kalimantan, Indonesia. Source of image is through tmap (Tennekes, 2018) in R from Esri World Imager, Open Street Map, Stamen Terrain and Carto Dark Matter. The section in red highlights the area that will be used to generate a canopy height model.

2.2 Overall Methodology

For this study, four different sets of data were created to be compared. This included Planet Lab's PlanetScope data at 3 m and 10 m resolution, Sentinel-2 data at 10 m resolution and the combination of both Sentinel 2 and PlanetScope data at 10 m resolution. Each of these datasets were then fed into three different machine learning algorithms (MLR, RF and CNN). The following sections will outline the overall methodology. The overall methodological approach employed to model and map canopy height for the combined dataset is illustrated in Figure 2. Each of the datasets included spectral bands, calculated vegetation indices, a Digital Terrain Model from Copernicus and associated topographic metrics (slope, aspect, terrain ruggedness index root mean square difference) and the Canopy Height calculated from airborne LiDAR data. The corresponding code is available on GitHub (Appendix 1), and an overview of data size for each data table (PlanetScope 3 m, 10 m, Sentinel-2 and Combined Data) is in Appendix 2.

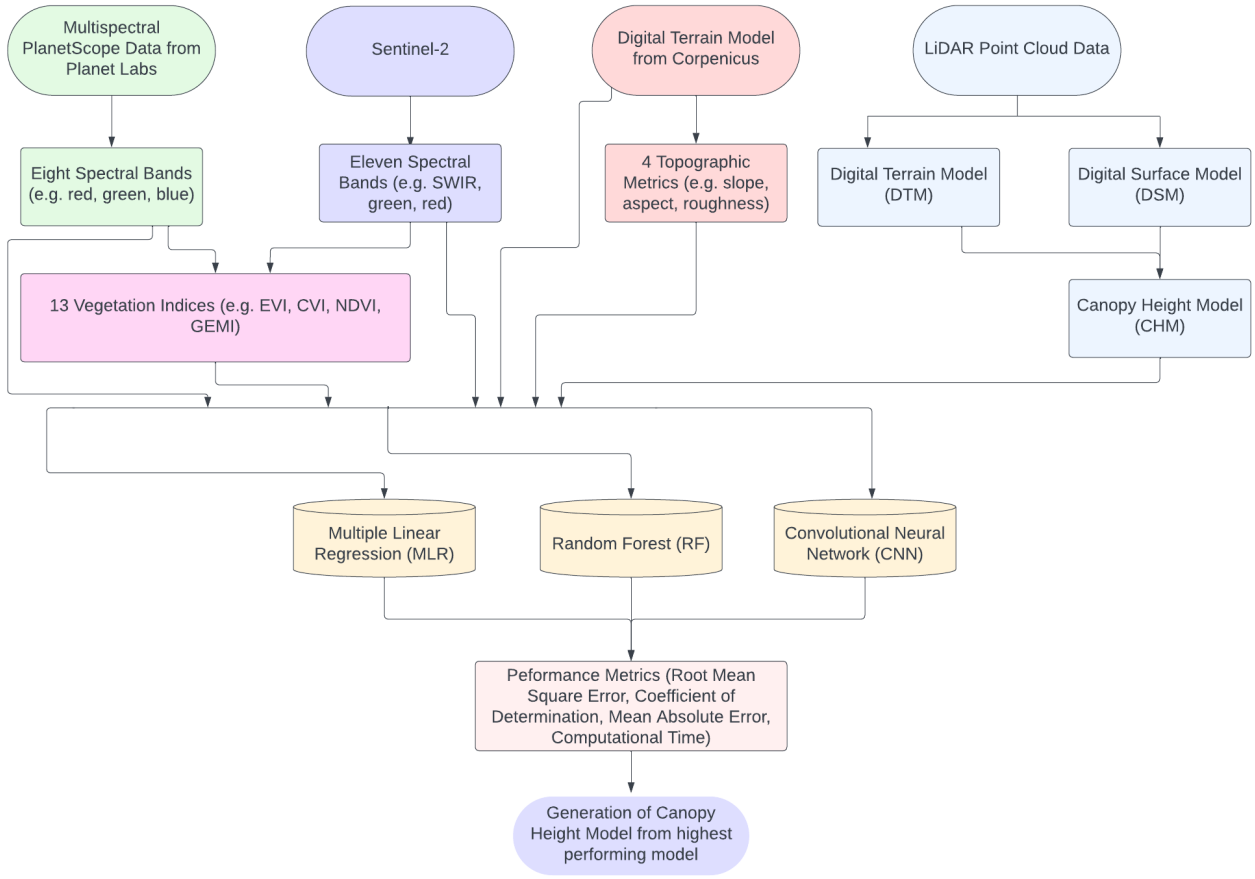

Figure 2. Methodological flowchart for modelling canopy height within the Katingan Mentaya Project using ALS, PlanetScope and Sentinel-2 Data at 10m resolution supplied to three machine learning algorithms (Multiple Linear Regression, Random Forest, and Convolutional Neural Network). Note abbreviations: Enhanced Vegetation Index (EVI), CVI (Chlorophyll Vegetation Index), NDVI (Normalised Difference Vegetation Index), GEMI (Global Environment Monitoring Index).

2.3 Software

In order to enhance the potential for future project reusability, this study utilised Free and Open Source Software (FOSS) whenever appropriate and accessible. FOSS solution harness the advantages of community-driven development and maximise reusability of workflows in future projects by Permian Global and by others across the industry. This approach promotes the sharing of knowledge and resources, facilitating a more seamless transfer of methodologies and tools between projects and people. All modelling techniques were performed using R Statistical Software (v4.3.0 R Core Team, 2022) and completed on an Ubuntu 22, which consisted of a Dual Intel Core Xeon Gold 5218, with a total of 768 GB of RAM (12 x Samsung 64 GB Load-Reduced DDR4 266 Mhz ECC Server Memory Module).

2.4 Airborne LiDAR Dataset

The airborne LiDAR survey was undertaken in August 2022 by PT Map Tiga Internasional (2022) within the southern region of the Katingan Mentaya Project, using a Leica DragonEye 1 MHz system with integrated IMU and Novatel L1/L2 GNSS antenna (PT Map Tiga Internasional, 2022). Accompanying digital imagery was captured with a ground pixel size of 15 cm. The average point densities for the project were < 11 points per m^2 for the overall density before classification, < 6 points per m^2 for the open bare ground and < 1 point per m^2 for the classified ground points under vegetation 25/08/2023 11:51:00. The LiDAR point cloud had a reported accuracy of +/- 0.15 m RMSE in the vertical (PT Map Tiga Internasional, 2022). From the classified LiDAR ground points, a Digital Terrain Model (DTM) and a Digital Surface Model (DSM) was generated to a resolution of 1 m x 1 m, by PT Map Tiga Internasional (2022). Both the DSM and DTM were derived using Terrascan software from the classified LiDAR ground points in 1 m cell resolution. Any tiles outside of the survey polygon were nulled (PT Map Tiga Internasional, 2022). The DTM and the DSM files were provided in GeoTIFF format which were imported into R as a SpatRaster using the *terra* Package (v1.7-8 Hijmans, 2023). The DSM and DTM were used to calculate the Canopy Height Model (CHM = DSM – DTM) (Figure 3a,c, Figure 4). The area was then cropped to the region of the Katingan Mentaya Project shapefile, which was digitised by Permian Global (2023a).

2.5 Planet Lab's PlanetScope Data

PlanetScope is a set of satellite constellations that are operated by Planet Labs with worldwide daily coverage (Planet Labs, 2023a). PlanetScope images have a pixel size ranging from 3.7 m to 4.1 m which were resampled to 3m x 3 m resolution by Planet Labs (Planet Labs, 2023a; Sentinel-Hub, 2023a). For this study, data from Planet Labs was downloaded by Dr Hugh Graham, which included the mean value composite of images within the Katingan Mentaya Project from May 2022 and July 2022. This dataset was then cloud and shadow masked by Dr Hugh Graham by utilising the Usable Data Mask from Planet Labs (Planet Labs, 2023c, p. 2) The *clear confidence percent* field was

chosen, where every pixel is given a confidence of "clear" classification from 0 to 100, the threshold was set to 80, and any pixel that was below the threshold was removed. The dataset included the whole region of the project; however, the data was cropped to the extent of the LiDAR data, resulting in an area of 198.5 km^2 (Figure 3b). The dataset contains eight spectral bands: coastal blue, blue, green, green i, yellow, red, red-edge and near infrared (Table 1). From these spectral bands, Normalised Difference Vegetation Index NDVI was first calculated before scaling (Table 2). Then all spectral bands were scaled to integer values for computational efficiency, by dividing the values of the spectral bands by 10,000. From these spectral bands, a further 12 vegetation indices were calculated (Table 2). It is also noted that unlike the Sentinel-2 data, PlanetScope data is not always a free source of data for all locations, however, through the Education and Research programme as well as Norway's International Climate and Forest Initiative, high-resolution optical satellite imagery of the tropics is freely available.

2.6 Sentinel-2 Data

Sentinel-2 data was accessed using the SpatioTemporal Asset Catalog (STAC), which is an ecosystem to find, download and work with spatial temporal data using an Application Programming Interface (API) (STAC, 2023). This was used in combination with the packages gdalcube (v0.6.4, Appel et al., 2021) and the rstac (v0.9.2.4, Simoes et al., 2021) in R. The freely available Sentinel-2 Cloud-Optimised GeoTIFFs (COG) catalogue was accessed on the Amazon Web Service (AWS) and the corresponding STAC-API endpoint at: https://earth-search.aws.element84.com/v0. The STAC search was set to the coordinates of the LiDAR data, the date range was set to 01-01-2021 to the 31-12-2022, the resolution to 10 m x 10 m, and the scene level cloud cover was set to a maximum of 20%. The Sentinel-2 data contained a total of 12 bands, where six bands are also included within the PlanetScope dataset (coastal blue, blue, green, red, red-edge and near infrared) (Table 1). The other six bands included two more red-edge bands (2 and 3), another near infrared (NIR2), water vapour, a short-wave infrared (SWIR1) (Table 1), and a scene classification (SCL) algorithm. The clearest image with minimal cloud cover was chosen, which was on the 27-02-2021. The few clouds on the image were cloud and shadow masked using the Scene Classification (SCL) band from Sentinel 2, this included cloud shadows, cloud of medium and high probability and thin cirrus clouds. The dataset was then cropped to the Katingan Mentaya Project shapefile (Figure 3d). The NDVI was then calculated and the SCL was removed, as this was only needed for detection of clouds. This resulted in 11 spectral bands that were then scaled to integer values for computational efficiency, by dividing the values of the spectral bands by 10,000. From these spectral bands, a further 12 vegetation indices were calculated (Table 1).

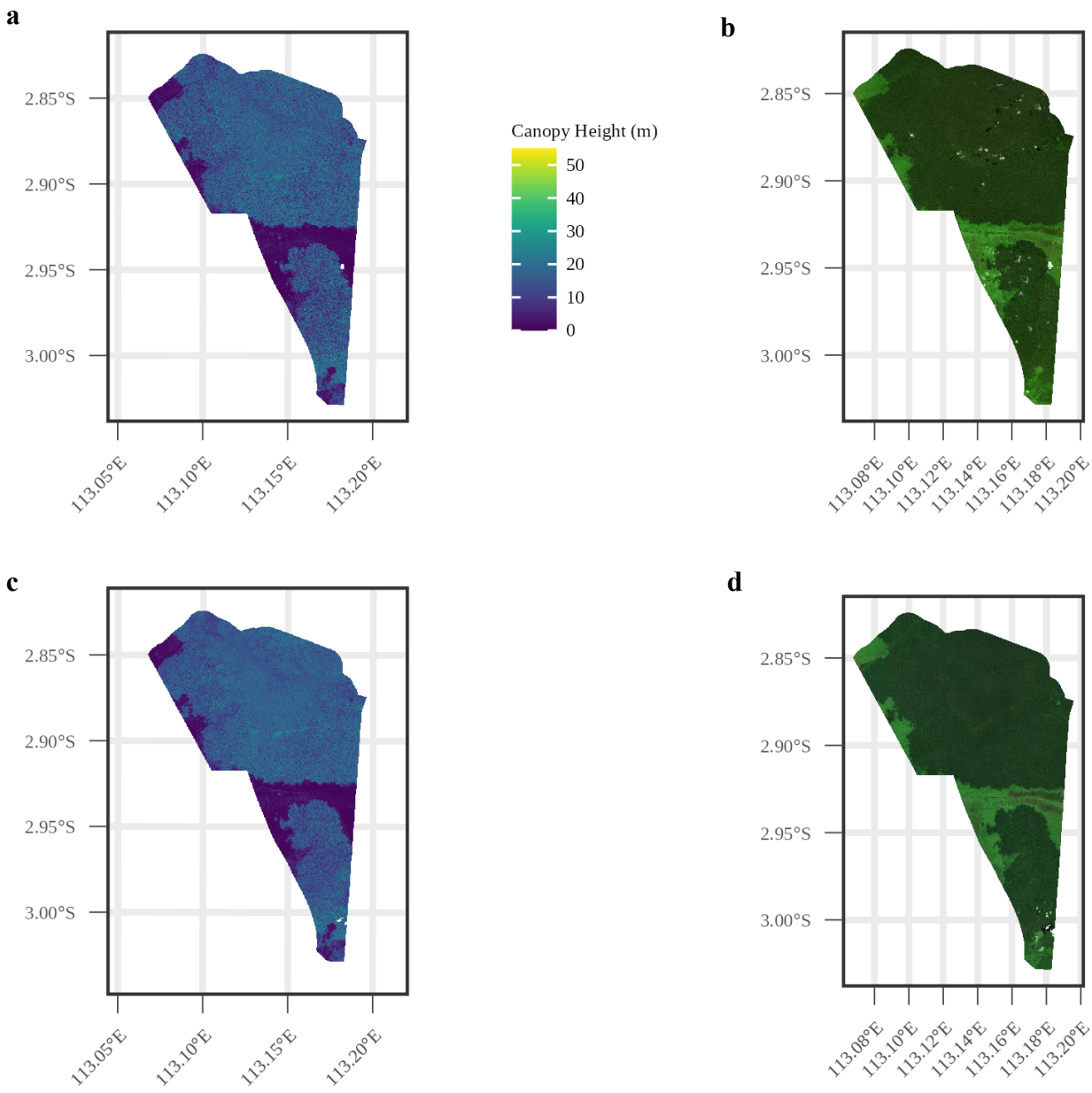

Figure 3. Canopy Height Model (CHM) obtained from Digital Surface Model (DSM) and Digital Terrain Model (DTM) by LiDAR observation in August 2022 at **(a)** 3 m resolution and **(c)** 10 m resolution. **(b)** True colour image of mean value composite images from Planet Labs PlanetScope data collected in May and July 2022 at 3 m resolution**. (d)** True colour image of Sentinel-2 satellite image at 10 m resolution taken in February 2022. (b) and (d) are images after shadow and cloud masking. All images are within the Katingan Mentaya Project.

Table 1. Comparison between the main specifications of spectral bands of Sentinel-2 and PlanetScope data

Band Name	Sentinel-2		PlanetScope	
	Band Number	Wavelength (nm)	Band Number	Wavelength (nm)
Coastal Blue	1	433 - 453	1	431 - 452
Blue	2	458 - 523	2	465 - 515
Green I	-	-	3	513 - 549
Green	3	543 - 578	4	547 - 583
Yellow	-	-	5	600 - 620
Red	4	650 - 680	6	650 - 680
Red-edge 1	5	698 - 713	7	697 - 713
Red-edge 2	6	733 - 748	-	-
Red-edge 3	7	773 - 793	-	-
NIR1	8a	855 - 875	8	845 - 885
NIR2	8	785 - 900	-	-
Water Vapour	9	935 – 955	-	-
SWIR1	11	1565 - 1655	-	-

2.7 Digital Terrain Model

Topography has the ability to capture biophysical properties that can influence forest structure such as canopy height (Caughlin et al., 2016), and including these metrics in remote sensing has been shown to increase the prediction of forest structural attributes (Anderson et al., 2008). Therefore, an open-source digital terrain model was downloaded and four topographic metrics were calculated including roughness, aspect, slope and the Terrain Ruggedness Index root mean square difference (TRIrmsd) using the terra package in R (v1.7-8 Hijmans, 2023) (Table 2). Although a digital terrain model was provided from the point cloud LiDAR data this was only be used in calculating the canopy height model and was not supplied to the machine learning pipelines, this increases the reproducibility of the models, allowing for the upscaling of the LiDAR data.

The DTM tiles were obtained from the Copernicus Digital Elevation collection with global coverage at a resolution of 30 m (European Space Agency, 2023b), accessed via the Microsoft Planetary Computer STAC catalogue https://planetarycomputer.microsoft.com/api/stac/v1 using R packages rstac (v0.9.2.4, Simoes et al., n.d.) and terra (v1.7-8 Hijmans, 2023). The search set to the coordinates of the LiDAR data and from this the topographic metrics were then calculated (Table 2).

Table 2. Description of vegetation indices and topographic metrics from Copernicus DTM

Source	Variables	Description
Copernicus Digital Terrain Model	Slope	Slope calculated from DTM
	Aspect	Aspect calculated from DTM. If slope = 0, aspect is set to 90 degrees
	Roughness	Roughness calculated from DTM is the difference between the maximum and the minimum value of a cell and its eight surrounding cells.
	Digital Terrain Model	Topographic model of the bare earth, acquired from Copernicus
	Terrain Ruggedness Index – root mean square difference (TRIrmsd)	TRIrmsd computes the square root of the mean of the squared differences between these cells
Sentinel-2 Data and PlanetScope Optical Data Spectral Bands	Normalized Difference Vegetation index (NDVI) (Rouse et al., 1974)	(N-R)/(N+R)
	Normalised Difference Red-Edge Index (NDREI) (Gitelson and Merzlyak, 1994)	(N – RE)/(N+RE)
	Enhanced Vegetation Index (EVI) (Huete, 1997)	2.5 * (N) – R/ (N) + 6 x(R) – 7.5 x(B) + 1
	Advanced Vegetation Index (AVI) (Rikimaru et al., 2002)	$(N \times (1.0 - R) \times (N - R)^{(1/3)}$
	Renormalised Difference Vegetation Index (RDVI) (Roujean and Breon, 1995)	$(N-R)/ ((N+R)^{0.5})$
	Chlorophyll Index – Red-Edge (CIRE) (Gitelson et al., 2003)	(N/RE) -1
	Green Normalised Difference Vegetation Index (GNDVI) (Gitelson et al., 1996)	(N – G)/ (N+G)
	Red Green Blue Vegetation Index (RGBVI) (Bendig et al., 2015)	$(G^{2.0} – B \times R)/ (G^{2.0} + B \times R)$
	Blue Normalised Difference Vegetation Index (BNDVI) (Wang et al., 2007)	(N – B)/ (N + B)
	Chlorophyll Vegetation Index (CVI) (Vincini and Frazzi, 2011)	$(N \times R)/ (G^{2.0})$
	Green-Blue Normalised Difference Vegetation Index (GBNDVI) (Wang et al., 2007)	(N – (G + B))/(N + (G + B)
	Green Leaf Index (GLI) (Louhaichi et al., 2001)	(2.0 x G – R – B)/(2.0 x G + R + B)
	Global Environment Monitoring Index (GEMI) (Pinty and Verstraete, 1992)	$((2.0 \times ((N^{2.0}) – (R^{2.0}) + 1.5 \times N + 0.5 \times R)/ (N + R + 0.5)) \times (1.0 – 0.25 \times ((2.0 \times ((N^{2.0}) – (R^{2.0}))$

2.8 Pre-Processing

To create the merged data for all three machine learning algorithms, the spectral bands, vegetation indices, topographic metrics and the canopy height model all needed to be the same resolution. All resampling was completed in R using the terra package feature "project" with bilinear interpolation. The spectral bands, vegetation indices, topographic metrics were set as the input features of the model, and the calculated canopy height from the LiDAR data was set as the target variable. Each model contained the same number of calculated vegetation indices (13) and the same number of topographic metrics (5); however, they had varying numbers of spectral bands. Although the data collected from Planet Labs, Sentinel 2, and LiDAR were not collected within the same time period, it was assumed that there was little to no variation with vegetation height over the 18-month period.

2.9 Data Table Processing for PlanetScope 3 m Resolution

The PlanetScope spectral bands and calculated vegetation indices were provided at a resolution of 3 m. The topographic metrics (DTM, aspect, slope, roughness, TRIrmsd) were increased from 30 m resolution to 3 m. The canopy height was then down sampled from 1 m resolution to 3 m resolution, resulting in canopy heights ranging from 0.01 to 47.59 (Figure 3a, Figure 4). The PlanetScope spectral bands (eight), calculated vegetation indices (13) and topographic metrics (five) were then merged as the 26 input features for the machine learning algorithms.

2.10 Data Table Processing for PlanetScope 10 m Resolution

To decrease the resolution of the PlanetScope data, the spectral bands and calculated vegetation indices were decreased from 3 m to resolution to 10 m resolution, using the same approach. The topographic metrics were increased from 30 m resolution to 10 m resolution. The canopy height calculated from LiDAR data was reduced from 1 m resolution to 10 m resolution, resulting in canopy heights ranging from 0.11 to 41.39 m (Figure 4). This resulted in 26 input features for the machine learning algorithms, including eight spectral bands, 13 calculated vegetation indices, and five topographic metrics.

2.11 Data Table Processing for Sentinel-2 10 m Resolution

The Sentinel-2 data was downloaded at a resolution of 10 m. Therefore, the spectral indices and calculated vegetation indices were already at this resolution. The topographic metrics were increased from 30 m resolution to 10 m resolution. The canopy height calculated from LiDAR data was reduced from 1 m resolution to 10 m resolution, resulting in the same canopy heights as seen in the PlanetScope data (Figure 3c, Figure 4). This resulted in 29 input features for the machine learning algorithms including 11 Sentinel-2 spectral bands, 13 calculated vegetation indices and five topographic metrics.

2.12 Data Table Processing for Combined Data of Sentinel-2 and Planet Scope 10 m Resolution

The spectral bands of Sentinel-2 that overlapped with PlanetScope's data (six) were renamed, and the topographic metrics and the canopy height model were removed from the Sentinel-2 10 m dataset. The PlanetScope 10 m resolution was then merged with Sentinel-2 dataset through the x and y coordinates. This resulted in a dataset containing 50 input features including 19 spectral bands (six of which were the same spectral bands from Sentinel-2 and PlanetScope), 26 calculated vegetation indices and five topographic metrics.

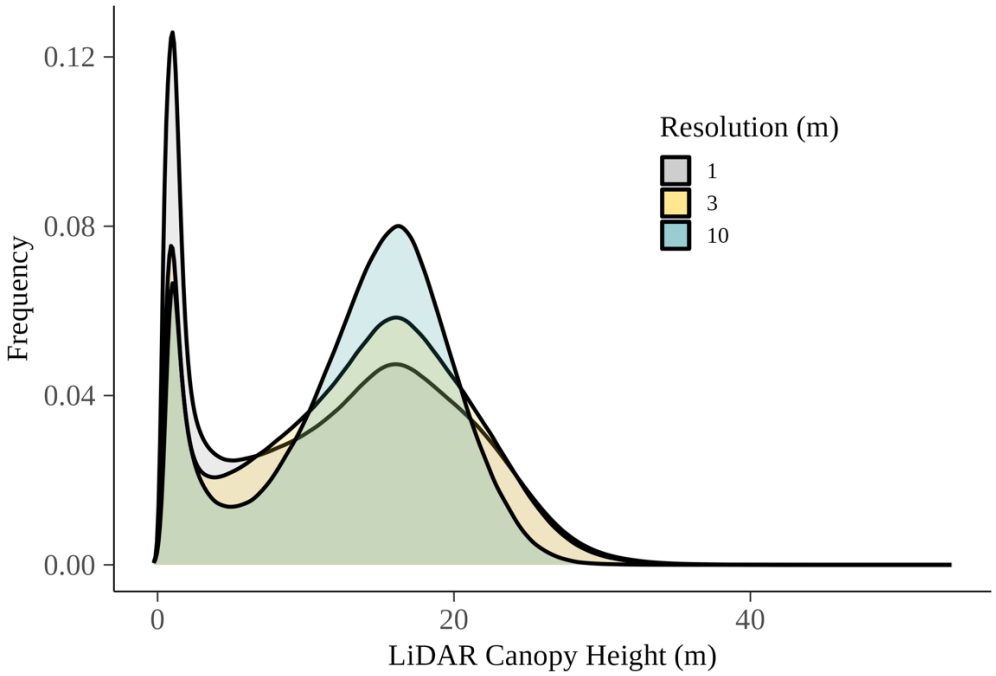

Figure 4. Density plot of canopy height derived from LiDAR survey in August 2022 at 1 m x 1 m resolution (grey), 3 m x 3 m resolution (yellow) and 10 m x 10 m resolution (blue).

2.13 Spatial Autocorrelation

When using remotely sensed data it is important to recognise and analyse spatial autocorrelation to reveal connections between neighbouring pixels due to sensor resolution and landscape variability (Congalton, 1988). Ignoring spatial autocorrelation may lead to false conclusions about relationships and inflate measures of accuracy during the modelling process (Veloz, 2009). Therefore, prior to the modelling process, the presence of spatial autocorrelation was assessed using Moran's I metric (Moran, 1950) and was also visualised through a variogram. The variogram was tested on a spatial resolution of 100 m (this was due to time, as even at 10 m, the variogram had not finished running after 15 hours). However, the Moran's I metric was tested on the original spatial resolution of LiDAR canopy height at 1 m and 100 m for comparison.

Moran's I metric is useful in quantifying the significance of the spatial autocorrelation in datasets (Hudak et al., 2002). The presence of a strong, positive spatial autocorrelation was indicated by the Moran's I result of 0.971 at 1 m resolution and 0.95 at 100 m resolution, suggesting that nearby locations tend to have similar canopy heights. Further to this, a variogram was also used to visually analyse the presence of autocorrelation (Figure 5). The variogram provided insights into the spatial structure and the relationship between the canopy heights at different distances, through three main parameters: the *nugget*, the *sill* and the *range*. The *nugget* is the semi-variance at zero and represents the measurement error, the *sill* represents the point at which the semi-variance plateaus and the *range* of a variogram is the lag distance at which the semi-variance reaches the sill value, and it is presumed that at this point autocorrelation is zero beyond the range (Bohling, 2005). As data exhibits greater spatial clustering, it is expected that the range will increase (Isaaks and Srivastava, 1989).The variogram was formulated by fitting a mathematical function to simulate the nugget, sill, range and therefore revealing the shape of the sample variogram (Hudak et al., 2002). These functions can be spherical, exponential, Gaussian and linear (Hudak et al., 2002). In this study, the variogram was simulated using an exponential model. The analysis revealed the nugget had a value of 0.021, the sill of 1.064 and the range of 3272.83 m, indicating that spatial autocorrelation extends up to approximately 3273 m. These finding highlighted the importance of accounting for spatial dependence in the subsequent modelling steps. Considering the substantial observed spatial autocorrelation, spatial resampling and cross validation were incorporated within the modelling process.

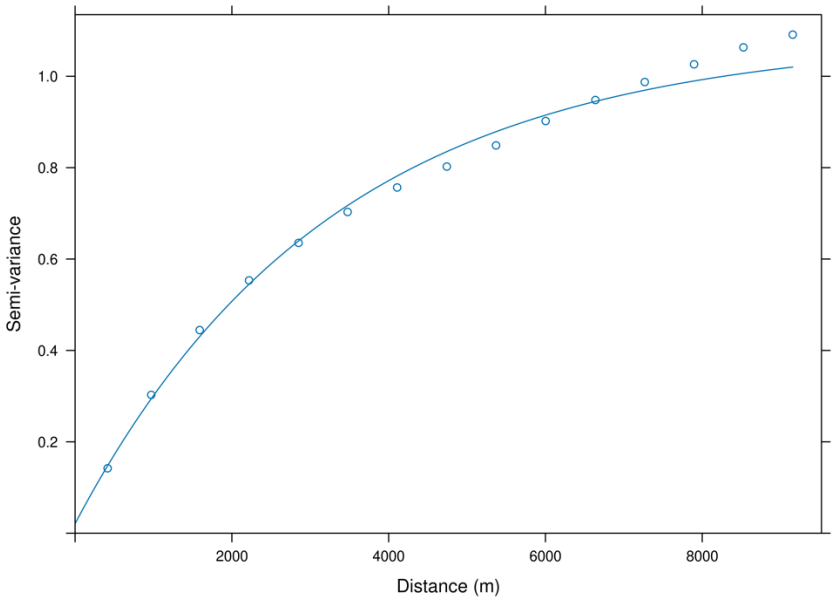

Figure 5. Spatial autocorrelation variogram of canopy height at 100 m resolution fitted with an exponential model within the Katingan Mentaya Project

2.14 Resampling Strategy – Spatial Cross-Validation

Spatial cross-validation (CV) has been demonstrated to yield more accurate model performance estimates than non-spatial methods (Mahoney et al., 2023). There have been numerous approaches for spatially assigning data to regions, and many of these have demonstrated improvements in performance estimates compared to randomised CV approaches (Mahoney et al., 2023). Mahoney et al. (2023) investigated which of the spatial cross-validation methods yield the most accurate estimates for model performance. This revealed that spatial clustering models are likely to yield the most accurate model performance estimates (Mahoney et al., 2023). Spatial clustering involves grouping observations into predefined number of clusters based on their spatial arrangement and offers considerable flexibility. Therefore, to determine the appropriate resampling strategy to account for spatial autocorrelation within canopy height, a repeated coordinate-based k-means clustering resampling plan (Brenning, 2012) was adopted within the mlr3 environment. This strategy splits data by clustering in the coordinate space and determines the appropriate number of folds, where each fold represents a distinct spatial coordinate region, and the number of times to repeat the resampling plan (Brenning, 2012). When using k-fold cross validation, it has been suggested that the appropriate number of k-fold is 10, as this demonstrates nearly unbiased results (Berrar, 2019; Simon, 2007). An exploratory analysis was carried out to see test the k-fold of 10 for this study area, where various folds were tested ranging from 2 – 10, and repeated twice, and the RMSE was observed (Figure 6). This was tested on the PlanetScope data at 10 m resolution using Multiple Linear Regression. The exploratory analysis demonstrated a decrease of error at 10 folds (Figure 6), therefore the resampling plan of all machine learning algorithms (MLR, RF, CNN) were set to 10 folds with 2 repeats. An example of the testing and training split with this resampling plan can be seen in Figure 7.

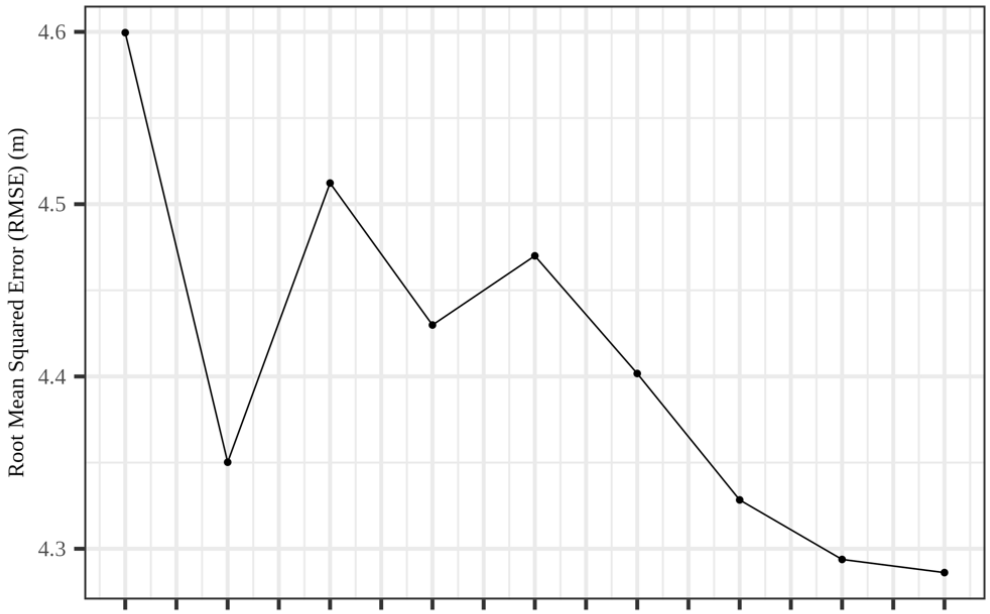

Figure 6. The resulting Root Mean Square Error (RMSE) when performing repeated coordinate-based k-means clustering resampling plan with Multiple Linear Regression on PlanetScope 10 m resolution. The number of folds range from 2 – 10, and the number of repeats set to two.

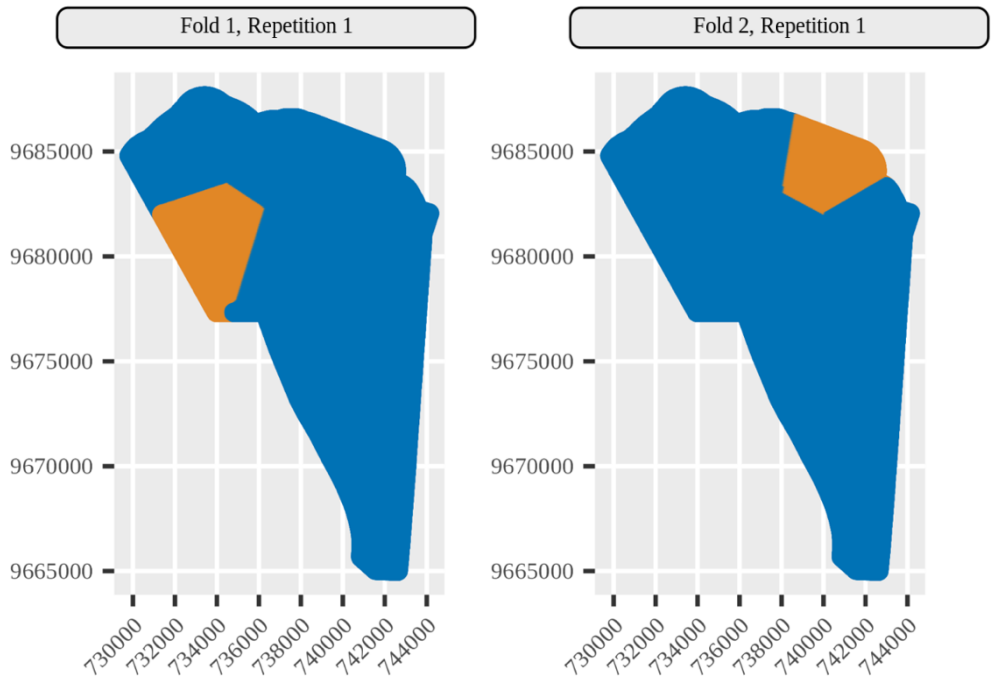

Figure 7. Two examples of the resampling plan of the train and test data within the Katingan Mentaya Project for one repetition. The resampling strategy includes 10 folds.

2.15 Multiple Linear Regression Model Building

Multiple Linear Regression is a widely used and straightforward supervised machine learning algorithm for predictive modelling. It offers simplicity in interpretation and is computationally less demanding compared to models incorporating neural networks. This type of parametric modelling has also been used extensively when modelling the relationship between remotely sensed data and various forest structures, with reasonable accuracy (Dubayah et al., 2010; Dube et al., 2015; Kulawardhana et al., 2014; Rischbeck et al., 2016; Torres de Almeida et al., 2022; Wang and Glenn, 2008).

The multiple linear regression model was developed using the mlr3 package (v0.16.1 M. Lang et al., 2019) in R. A filter strategy of "find_correlation" was implemented as a pre-processing step before implementing the MLR, allowing for a reduction in information redundancy and also assists in overfitting issues (Torres de Almeida et al., 2022). In this case, the "find_correlation" filter creates a correlation matrix between all features. If two features have a high correlation, the filter looks at the mean absolute correlation of each variable and removes the variables with the highest value. This gives each feature a value between 0 and 1, that is one minus the cut off value. In this case the cut off value was tuned in the mlr3 environment by looking at values better 0.3 and 0.8, where it removed features below the specified threshold. This was then iterated over 10 times to identify the optimal filter value. The resampling strategy was then initiated, followed by training the model using the selected features from the "find_correlation" filter. Finally, the testing data was tested, and the computational time was recorded.

2.16 Random Forest Model Building

Random Forest is an ensemble learning method that uses recursive partitioning to create multiple regression trees to make predictions (Breiman, 2001). The random characteristic of this method allows for increased stability of the model, and can enhance the robustness of the model (Zhang et al., 2022). Further to this, it is able to reduce overfitting as RF will take the average of the predicted values across the decision trees (Wang et al., 2021). Random Forest has been adopted widely for canopy height modelling and prediction, producing results of high accuracy (Csillik et al., 2020; Dube et al., 2015; Fassnacht et al., 2021; Fayad et al., 2021; Gupta and Sharma, 2023).

To model canopy height a random forest regression model was used. Ranger was implemented within the mlr3 environment (v0.16.1 M. Lang et al., 2019), which is fast implementation of RF particularly suited for high dimensional data (Breiman, 2001; Wright and Ziegler, 2015). Calibration of the model was divided into two stages; feature selection and hyperparameter tuning, which was completed on a subsample of the data due to time and computational constraints. This was originally tested on 300,000 pixels, however, using a subsample of the data set to 5% yielded very similar results, and took less time to complete (Table A3.1). Therefore 5% of each data source was used. Subsampling data is a common approach for RF modelling (Pourshamsi et al., 2021; Shimizu et al., 2020) For each RF model, feature selection took place through the implementation of importance = “impurity” in the mlr3 environment (Bergstra and Bengio, 2012). The feature selection process ranks the numerical features and extracts those features that are most important for predicting canopy height. This process of removing features that are of less importance, allows for training time to be reduced and decreases overfitting issues. The number of features to extract was then tuned between 30% of the features to 80%.

To find the optimum model for the RF, hyperparameter tuning took place through the implementation of a flexible Bayesian optimiser (mbo) (Schneider et al., 2023). This was chosen due to its ability to converge to a promising set of hyperparameters in fewer iterations compared to grid or random search. The following hyperparameters were then tuned: the number of features to split at each node (mtry), the fraction of data to be used for growing each tree (sample.fraction), the minimum node size (min.node.size), and whether the sampling in the bootstrap aggregation sampling is done with or without replacement (replace). By decreasing the number of mtry, it increases the number of random feature selection, which can help to prevent overfitting; however, a larger value can lead to more feature diversity, potentially capturing more complex patterns but increasing the risk of overfitting. Sample fraction specifies the proportion of the training data to be used for constructing each decision tree. Setting the sample fraction to 1.0 means that all training data are used, a lower value will randomly select a sample of the data. Smaller values introduce more randomness, which can help prevent overfitting and improve generalisation. However, if it set too low, it might lead to underfitting and reduced model performance. Finally, using replacement helps to introduce more randomness and

diversity, with can lead to better generalisation. Once the optimal model was selected, the features and hyperparameters were extracted and the resampling strategy was initiated, followed by training of the data. All hyperparameter tuning results for each model can be found in Table A3.2. The number of trees for all models was set to 500.

2.17 Convolutional Neural Network Model Building

Convolutional Neural Networks (CNNs) have provided a new set of tools for research within the remote sensing field due to their ability to process large amounts of training data with more accurate predictions, as well as their ability to effectively capture spatial information and exploit the correlation between neighbouring pixels (Shah et al., 2020). A CNN consists of several key elements: convolutional layers, pooling layers, dropout layers, and fully connected layers. Convolutional layers employ small filters, known as kernels, that slide along the input array, detecting patterns in the data and learning to extract significant features. Pooling layers contribute to spatial dimension reduction in the features maps, which aids in reducing computational complexity and the risk of overfitting. Lastly, fully connected layers, also known as dense layers, flatten the extracted features for further processing.

In this study a 2D-CNN was developed using the Keras (v 2.11.1 Chollet and Allaire, 2017) framework with the TensorFlow (v.2.11.0) backend in R. The first step involved normalising all features and the canopy height model between 0 and 1. This not only speeds up the convergence of training, but also ensures that each feature channel has the same magnitude which means that the parameter regularisation within the CNN affects each feature equally (N. Lang et al., 2019). Next, various configurations of the CNN was trialled and tested, which resulted in a network which takes in a 10 x 10 x N matrix as input, where N is the total number of features. Both 20 m x 20 m and 30 x 30 m were also tested, however these needed more than 500 GB of Random Access Memory (RAM) for the creation of the array, and either crashed or did not result in any increase in performance. The first layer within the Convolutional Neural Network adds 32 convolutional layers, each having a kernel size of 3 x 3, and a rectified linear unit (ReLU) activation function. This is followed by a 2D max-pooling layer with a pool size of 2 x 2. This helps reduce the spatial dimensions of the output from the previous convolutional layer. This is then fed into a drop out layer, with a dropout rate of 0.1, preventing overfitting by randomly setting a fraction of input units to 0 during training. Another 2D Convolutional layer and max pool layer block, but this time 64 filters are included in the convolutional layer. This is then passed onto a layer flatter function, which flattens the 3D output to a 1D vector, preparing it for the fully connected layers. There are two fully connected layers, where the first layer has 128 neurons which helps capture complex patterns within the data. It is finally passed to the final fully connected dense layer has a value of 1 unit and a linear activation function. This linear activation function is used for regression tasks to allow the model to predict continuous values, which

in this case is canopy height. The model's complexity was constrained due to time and computational constraints (e.g. an extra layer was added to the model, which required double the amount of time). The model was compiled using a popular variant of stochastic optimisation called "ADAM", due to its low memory requirement and its ability to adaptively adjust learning rates and momentum to speed up convergence during training (Kingma and Ba, 2014). Training was then activated, with 50 epochs, and a batch size of 64. Various batch sizes were tested, with 64 resulting in the more accurate predictions. The compiled model also used 10% of the training data for validation. Additionally, an early-stopping call-back was used to monitor the validation error and training was stopped if there was no improvement in the validation mean absolute error after 15 epochs to prevent overfitting issues and also saves computational time. The loss on the validation set was regularly observed over the training iterations to check for overfitting and underfitting (Figure A3.1). This was then iterated over the resampling strategy.

2.18 Performance Metrics

Mean Absolute Error (MAE), Root Mean Square Error (RMSE) and Coefficient of Determination (R-squared) were calculated to assess the predictive performance of all the three machine learning algorithms and the corresponding models of PlanetScope (3 m, 10 m), Sentinel-2 and combined PlanetScope and Sentinel-2. This was completed after the resampling strategy of repeated-coordinate k-means cross-validation strategy had taken place, and the combined prediction of all individual resampling iterations were averaged, this is known as micro-averaging. The computational time (minutes) was also recorded which was the total time taken for tuning, training, and the repeated-coordinate k-means cross-validation strategy, for each of the models.

3. Results

3.1 Accuracy Assessment of Multiple Linear Regression Model

Multiple linear regression was used as a base model to predict canopy height within the Katingan Mentaya Project. A total of four multiple linear regression models were developed based on features from PlanetScope 3 m and 10 m resolution, Sentinel-2 data 10 m resolution, and a combination of both PlanetScope and Sentinel-2 at 10 m resolution. The accuracy of estimating canopy height derived from LiDAR of each model was evaluated.

PlanetScope data was tested at both 3 m resolution and 10 m resolution, where 26 features were inputted into the model and using "find_correlation" only a subsample of the features were extracted to be used in the training process (Table 3). The PlanetScope 10 m resolution data, the Sentinel-2 data and the combined dataset all completed training under 5.5 minutes; however, the PlanetScope 3 m resolution took a total of 34.41 minutes (Figure 12, Table A3.3). The highest performing model was the Sentinel-2 data, where a total of 29 features were fed into the model, but only 18 features were

selected (Table 3), resulting in an MAE of 2.89 m, RMSE of 3.70 m and an R^2 of 0.65 (Figure 12, Table A3.3). This was then followed by the combined dataset where 25 features were selected (MAE = 2.90 m, RMSE = 3.73 m, R^2 = 0.64), the PlanetScope at 10 m resolution where 11 features were selected (MAE = 3.48 m, RMSE = 4.40 m, R^2 = 0.50) and finally the PlanetScope 3 m resolution where 15 features were selected (MAE = 4.61 m, RMSE = 5.76 m, R^2 = 0.37). The underestimation of the canopy height in higher canopy height was observed in all MLR models, and all models tended to predict canopy heights with values that were below zero (Figure 13a, Figure 15a, Figure 17a, Figure 19a).

Table 3. Features extracted for Multiple Linear Regression Models to Predict Canopy Height

Data Source	Score	Features	Data Source	Score	Features
PlanetScope (3 m)	0.60	BNDVI CIRE CVI GBNDVI NDVI RDVI RGBVI Aspect Blue Coastal Blue DTM Red Red-Edge Slope Yellow	Sentinel-2 (10 m)	0.61	BNDVI CIRE CVI GBNDVI NDVI RDVI RGBVI SWIR 11 SWIR 9 Aspect Blue Coastal Blue DTM Green Red Red-Edge Slope VNIR 8
PlanetScope (10 m)	0.42	BNDVI CIRE CVI RDVI RGBVI Aspect Blue Coastal Blue DTM Green I Slope	Combined Planet Scope (PS) and Sentinel-2 (S2) (10m)	0.44	BNDVI (PS) CIRE (PS) CIRE (S2) CVI (PS) CVI (S2) EVI (S2) GBNDVI (PS) GBNDVI (S2) GNDVI (PS) GNDVI (S2) NDVI (S2) RDVI (PS) RDVI (S2) RGBVI (PS) RGBVI (S2) SWIR 11 (S2) Aspect Blue (PS) Blue (S2) Coastal Blue (PS) Coastal Blue (S2) DTM Green (S2) Red (S2) Slope

3.2 Accuracy Assessment of Random Forest Model

A total of four random forest models were developed based on features from PlanetScope 3 m and 10 m, Sentinel-2 data 10 m resolution, and a combined dataset of both PlanetScope and Sentinel-2 at 10 m resolution. The accuracy of estimating canopy height derived from LiDAR data was evaluated.

When performing RF to predict canopy height, the importance filter provided varying features for each model; however, green and red-edge were ranked within the top two most important features, regardless of spatial resolution or data source (Figure 8 – 11). The data sources of 10 m resolution (PlanetScope, Sentinel-2, and combined) all completed hyperparameter tuning, cross validation and training in under 35 minutes, whereas the PlanetScope at 3 m resolution took a total of 450 minutes to run. The highest performing data source was from the combined data of PlanetScope and Sentinel-2 at 10 m resolution, with an R^2 of 0.69, an RMSE of 3.47 m and an MAE of 2.58 m (Figure 12, Table A3.3). The Sentinel-2 10 m resolution had a similar performance with an R^2, RMSE and MAE of 0.68, 3.52 m and 2.63 m, respectively (Figure 12, Table A3.3). This was then followed by the PlanetScope 10 m resolution (R^2 of 0.60, RMSE of 3.97 m and MAE of 3.01 m), and finally the PlanetScope 3 m resolution (R^2 of 0.43, RMSE of 5.50 m and MAE of 4.27 m) (Figure 12, Table A3.3).

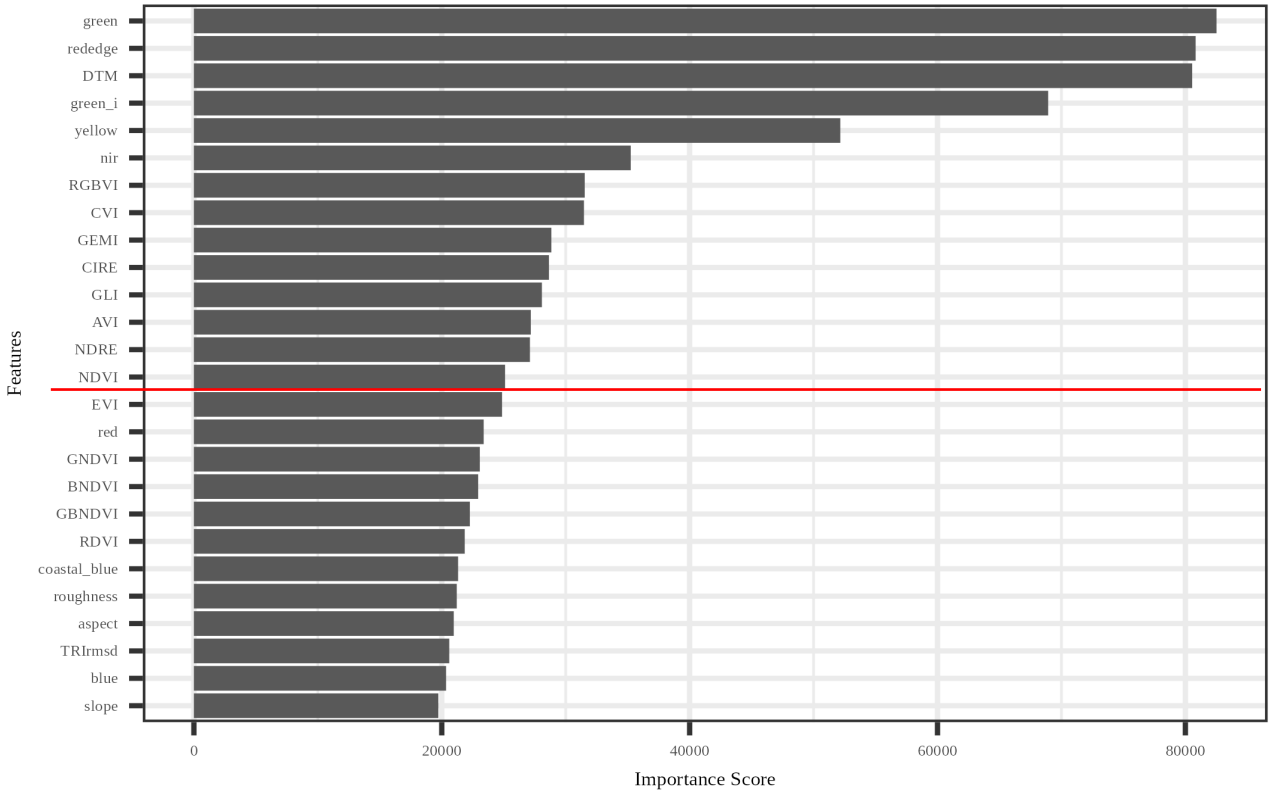

Figure 8. Feature importance score for PlanetScope at 3 m x 3 m resolution. Features above the red line were used within the Random Forest model to predict canopy height.

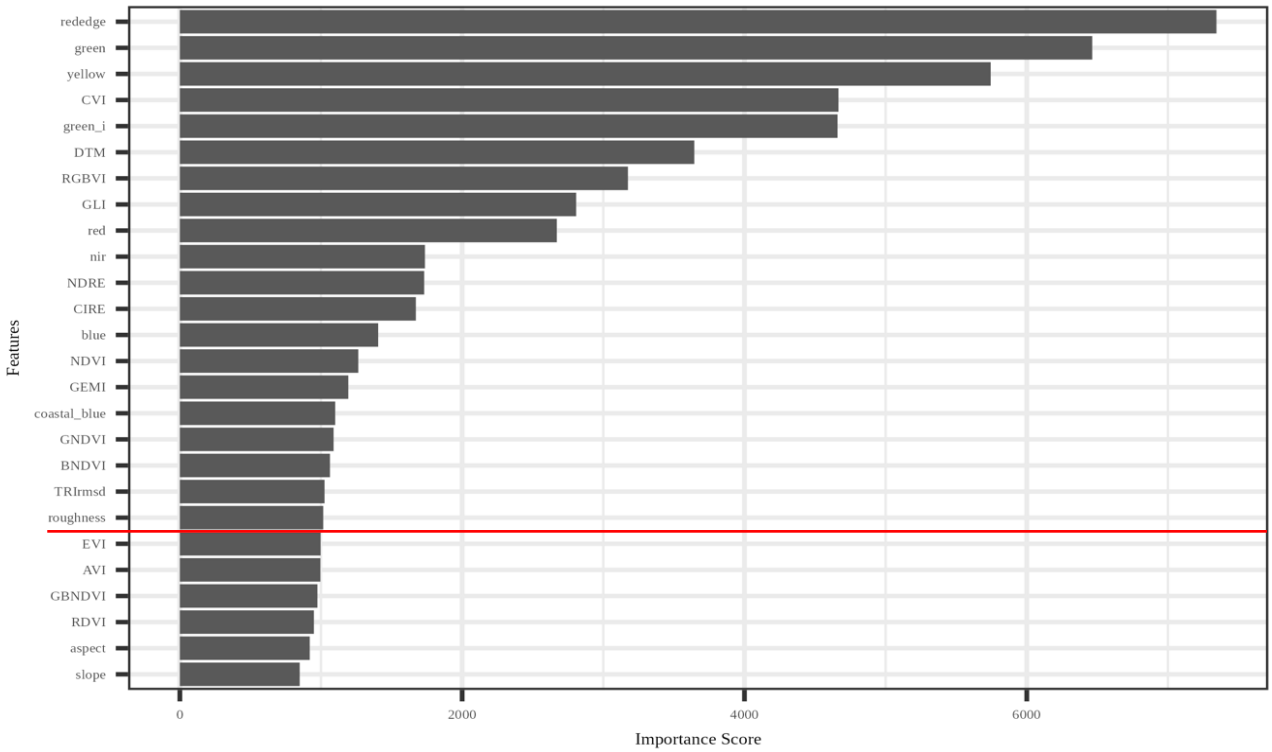

Figure 9. Feature importance score for PlanetScope at 10 m x 10 m resolution. Features above the red line were used within the Random Forest model to predict canopy height.

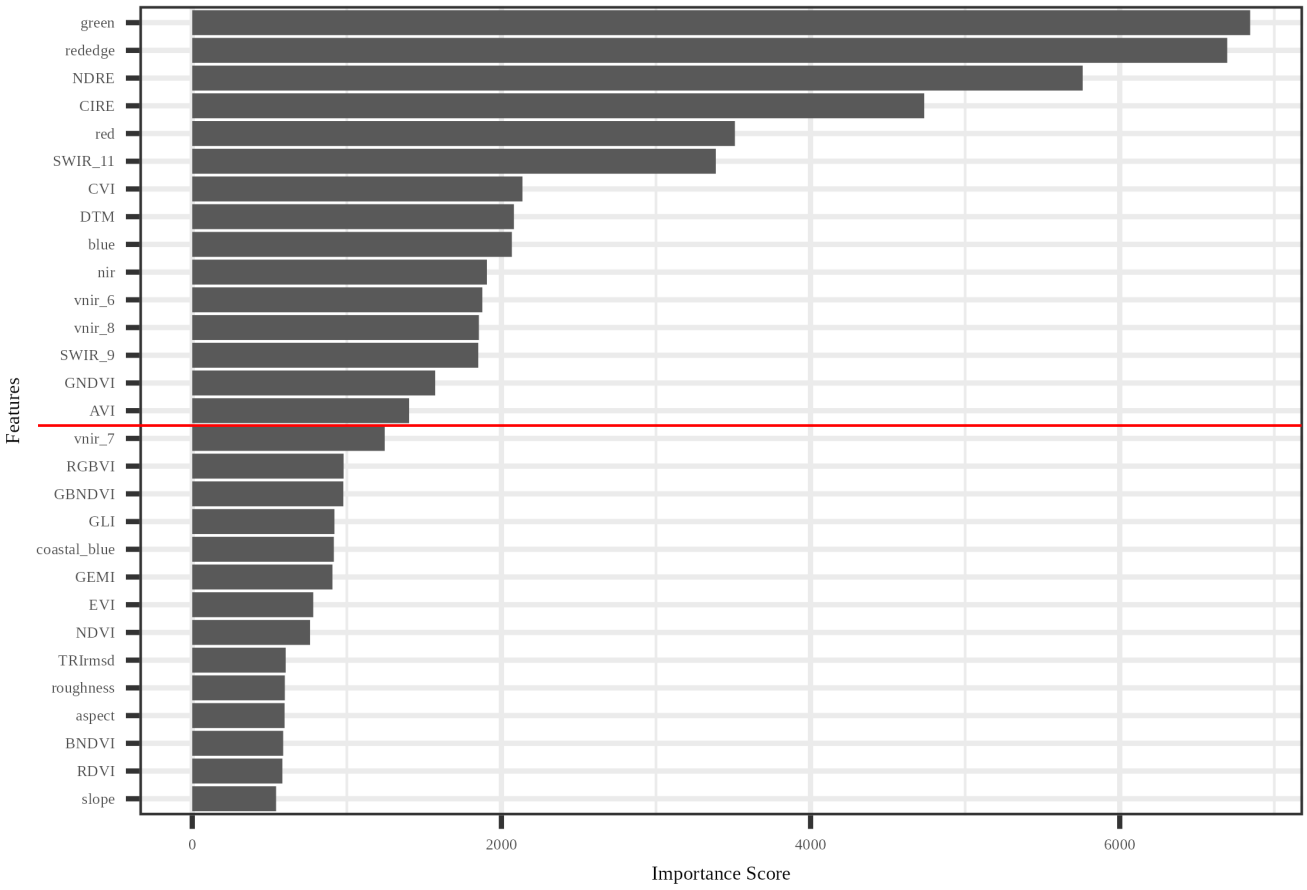

Figure 10. Feature importance score for Sentinel-2 at 10 m x 10 m resolution. Features above the red line were used within the Random Forest model to predict canopy height.

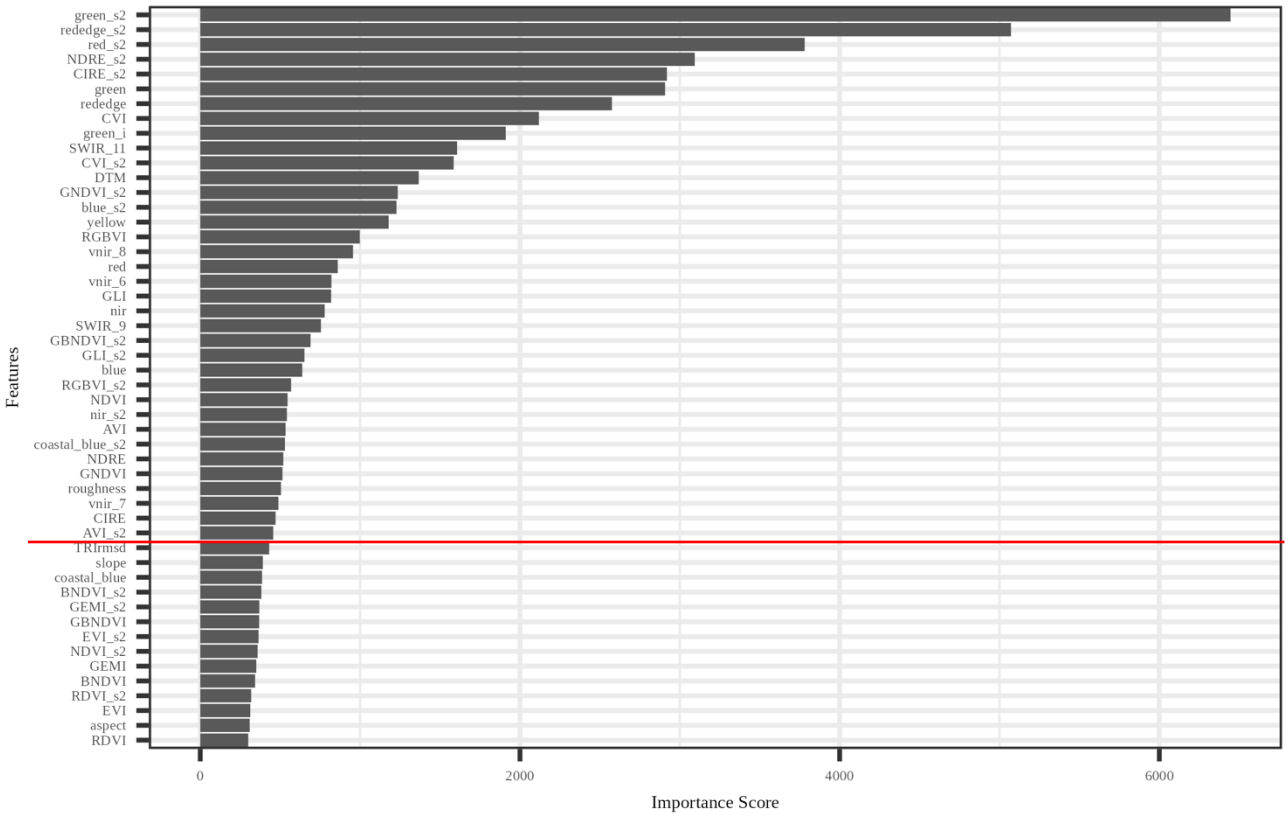

Figure 11. Feature importance score for combined data of both PlanetScope and Sentinel-2 data at 10 m x 10 m resolution. Features above the red line were used within the Random Forest model to predict canopy height.

3.3 Accuracy Assessment of Convolutional Neural Network Model

The CNN models were trained with all available features for each data source, with canopy height derived from LiDAR data as the target output. The network was trained to minimise the mean absolute error between prediction and the LiDAR CHM. Each model had varying computational time from 77 minutes for the Sentinel-2 data to 2723 minutes for the PlanetScope 3 m data. The difference in computation time was not only due to the size of the data source but was also due to the implementation of early stopping call back that was initiated during training. The highest performing model was the Sentinel-2 data which included a total of 29 features, providing an R^2 of 0.69, an RMSE of 3.47 m and an MAE of 2.64 m (Figure 12, Table A3.3). The combined data set which contained a total of 50 features had a similar performance with an R^2 of 0.68, an RMSE of 3.50 m and a MAE of 2.68 m. This was then followed by the PlanetScope 10 m resolution (R^2 of 060, an RMSE 3.95 m and MAE of 3.05 m), and finally the PlanetScope 3 m resolution (R^2 of 0.42, RMSE of 5.53 m and an MAE of 4.32 m) (Figure 12, Table A3.3), which both contained a total of 26 features.

3.4 Comparison of Canopy Height Models Derived using multiple data sources

In this study, a total of 12 models were developed based on varying data sources at different spatial resolutions: PlanetScope 3 m and 10 m resolution, Sentinel-2 10 m resolution and combined PlanetScope and Sentinel-2 at 10 m resolution. The accuracy of each model to estimate airborne LiDAR derived canopy height was evaluated using MAE, RMSE, R^2, and time (Figure 12). Overall, although multiple linear regression was the fastest machine learning algorithm, it had the lowest R^2 and the highest RMSE and MAE scores across all data sources. The Random Forest and Convolutional Neural Network had a similar performance across all data sources; however, the RF was the only model that did not predict values below zero (Figure 13, 15, 17, 19) and the CNN took much longer to run compared to that of the RF (Figure 12).

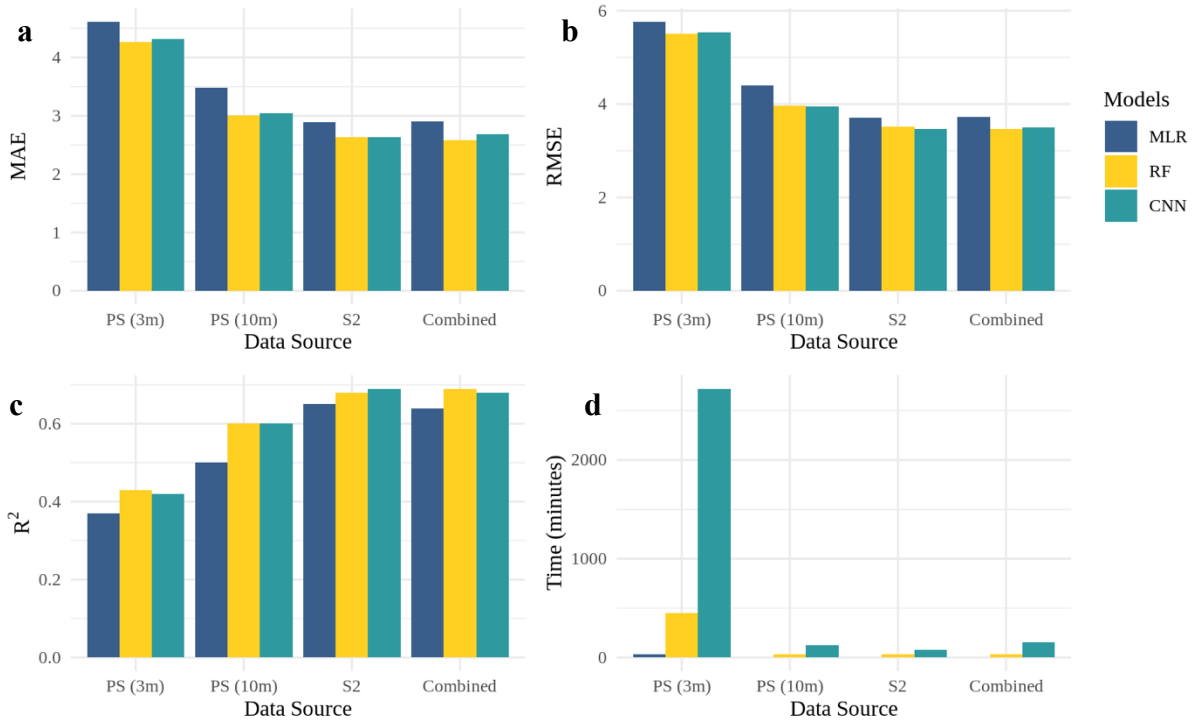

Figure 12. (a) Mean Absolute Error (MAE), **(b)** Root Mean Square Error (RMSE), **(c)** Coefficient of Determination (R^2), and **(d)** Time (mins) for three different machine learning algorithms; Multiple Linear Regression (MLR), Random Forest (RF), Convolutional Neural Network (CNN) from different combinations of optical data (PlanetScope (PS) 3 m, PS 10 m, Sentinel-2 (S2) 10 m, and combined PS and S2 at 10 m).

Overall, PlanetScope at 3 m resolution had the lowest performance, where for each machine learning algorithm (MLR, RF and CNN) the R^2 was consistently below 0.5 (Figure 13), and each model had the highest MAE and RMSE of the machine learning algorithms ranging from 4.27 – 4.61 m and 5.50 - 5.76 m, respectively (Figure 12, Table A3.3). Each machine learning algorithms were unable to predict many of the higher canopy heights within the region, where the majority of heights above 30 m were predicted as 25 m or below. The highest performing model for PlanetScope 3 m was the RF (Figure 14), however this was closely followed by the CNN. The CNN also tended to predict some of the canopy heights below 0 m, especially between 0 and 5 m (Figure 13c).

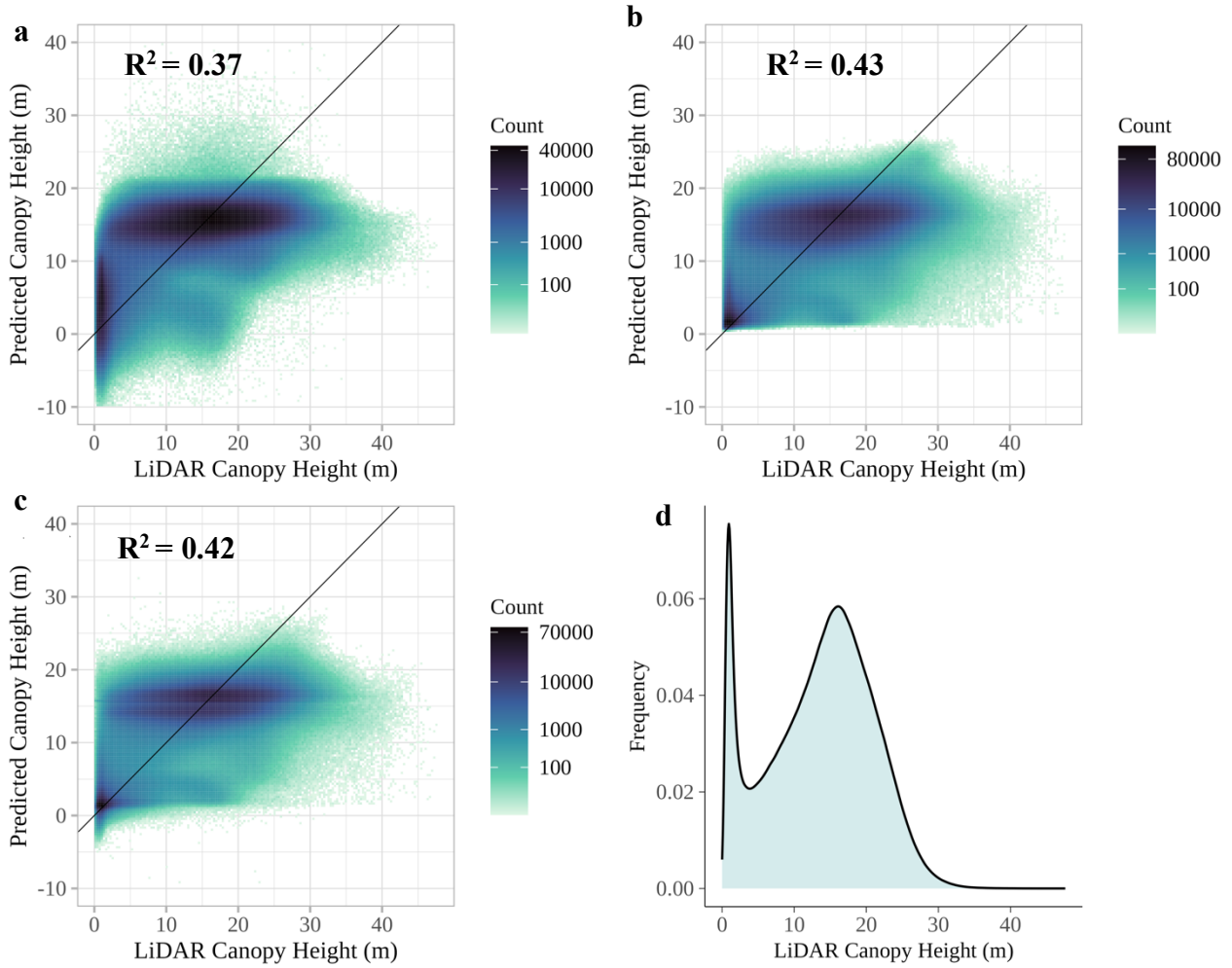

Figure 13. Scatterplots of predicted canopy height (m) for PlanetScope 3 m resolution using **(a)** Multiple Linear Regression **(b)** Random Forest, **(c)** Convolutional Neural Network. **(d)** Canopy Height Density plot of LiDAR derived canopy height at 3 m resolution for comparison. NB: To aid visualisation **(a)** is missing 774 rows of data, as they are not within the fixed y axis limits.

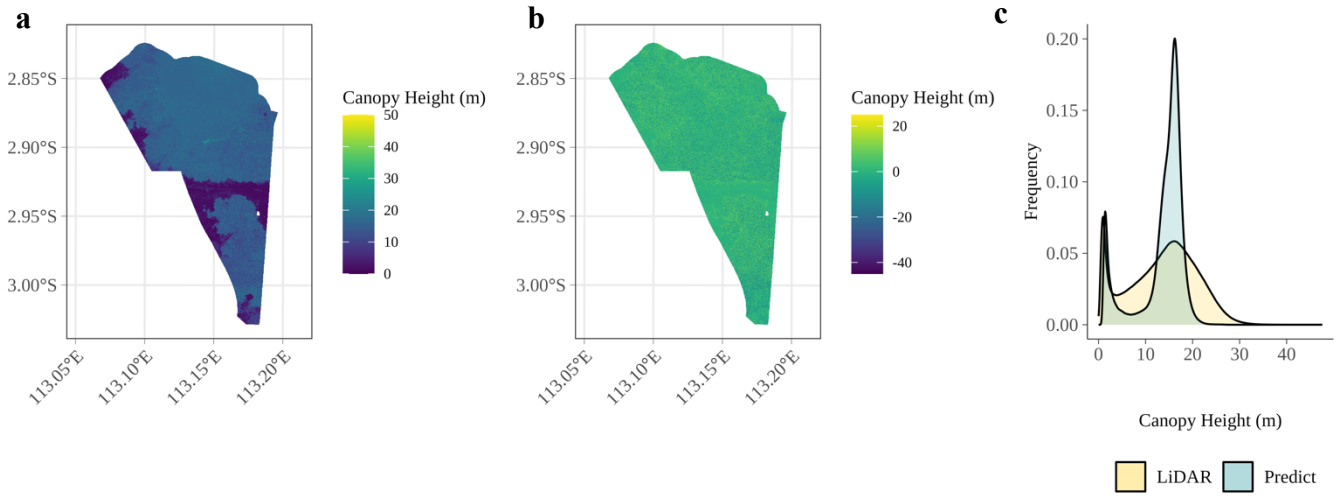

Figure 14. (a) Predicted Canopy Height Model from Random Forest for the PlanetScope 3 m resolution data **(b)** Difference between the Predicted Canopy Height and the LiDAR derived Canopy Height **(c)** density plot comparing the canopy height derived from LiDAR and the predicted canopy height (m).

The PlanetScope at 10 m resolution had a better performance to the higher resolution of 3 m, where the R^2 ranged from 0.50 for the MLR to 0.60 for both the RF and CNN (Figure 15). The RF and CNN had a very similar performance, with the same R^2, however, the CNN had a higher MAE at 3.05 m compared to 3.01 for the RF, but a lower RMSE at 3.95 m compared to 3.97 m for the RF. The PlanetScope at 10 m resolution did start to predict beyond 25 m for the CNN and RF. However, the majority of canopy heights beyond 35 m were only predicted as high as 20 m. The predicted Random Forest Canopy Height model for PlanetScope 10 m can be seen in Figure 16.

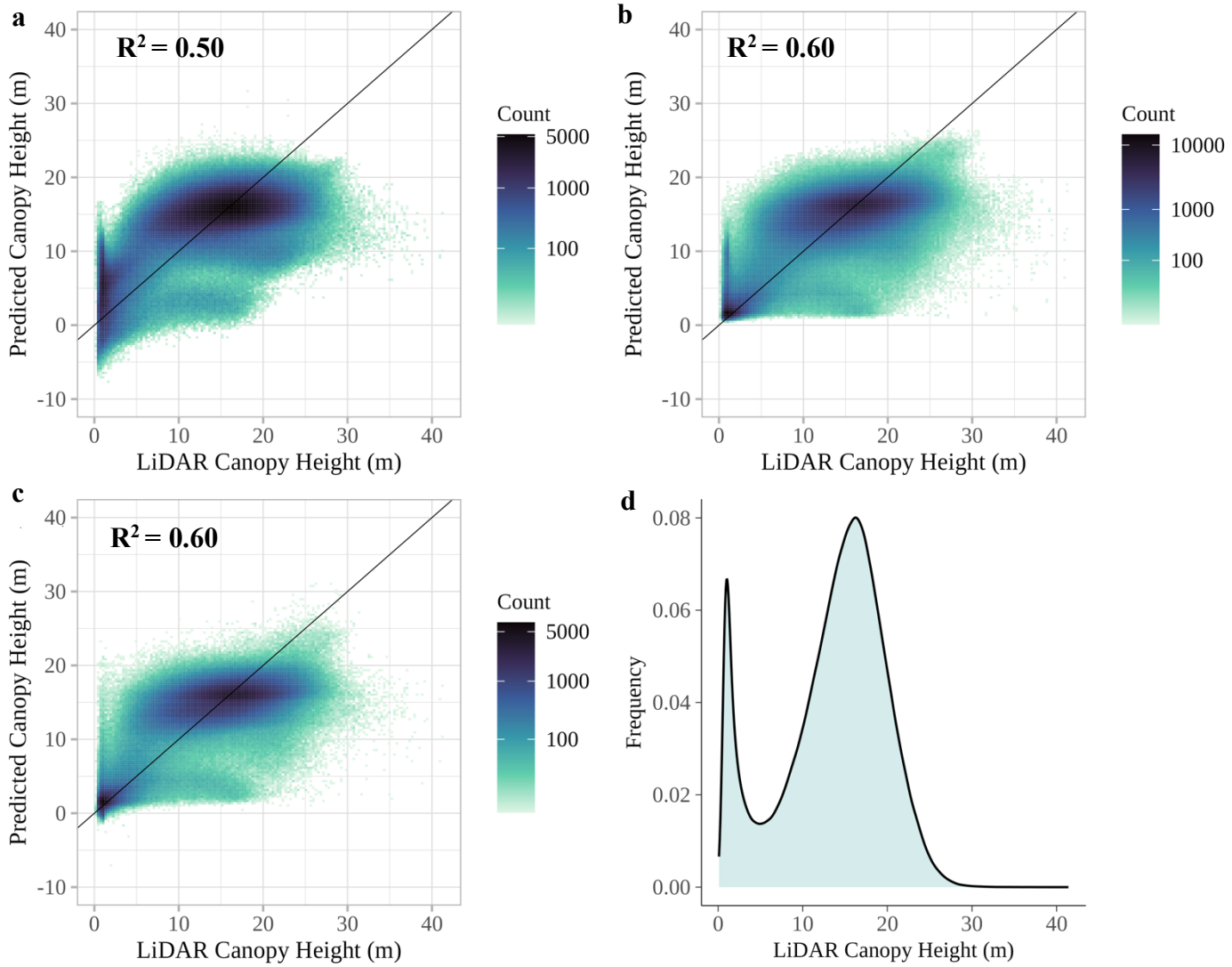

Figure 15. Scatterplots of predicted canopy height (m) for PlanetScope 10 m resolution using **(a)** Multiple Linear Regression **(b)** Random Forest, **(c)** Convolutional Neural Network. **(d)** Canopy Height Density plot of LiDAR derived canopy height at 10 m resolution for comparison.

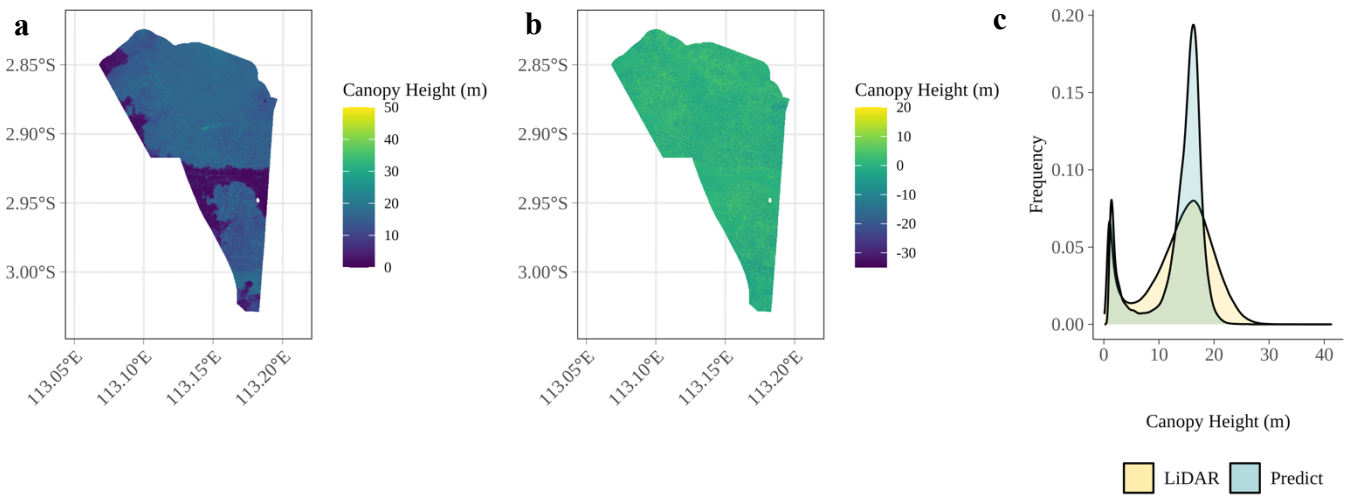

Figure 16. (a) Predicted Canopy Height Model from Random Forest for the PlanetScope 10 m resolution data **(b)** Difference between the Predicted Canopy Height and the LiDAR derived Canopy Height. **(c)** density plot comparing the canopy height derived from LiDAR and the predicted canopy height (m).

The Sentinel-2 and combined dataset had a similar performance for each machine learning algorithm (Figure 12, 17, 18). This demonstrates that the addition of all PlanetScope features with the Sentinel-2 did not make much difference in the models' ability to predict canopy height derived from LiDAR, where the combined dataset only had a slightly higher performance than the Sentinel-2 data with the CNN (Figure 12, 17, 18). The two highest performing models came from the CNN Sentinel-2 with an R^2 of 0.69, MAE of 2.64 m, RMSE of 3.47 m (Figure 18) and the RF of the combined data set which had the same R^2 and RMSE, but an MAE of 2.58 m (Figure 20). In both of these models some of the LiDAR canopy heights of 30 m were able to be predicted beyond 25 m.

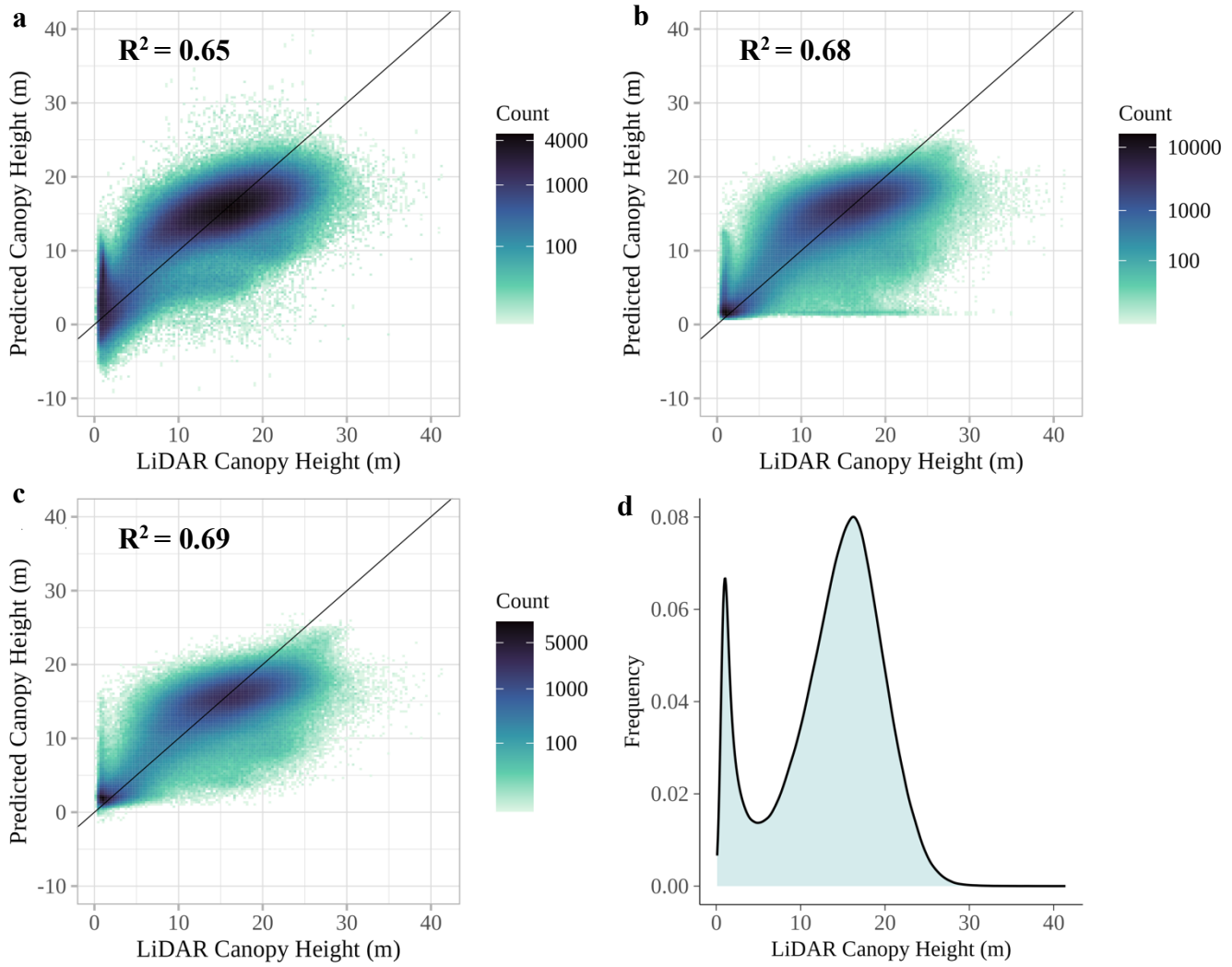

Figure 17. Scatterplots of predicted canopy height (m) for Sentinel-2 at 10 m resolution using **(a)** Multiple Linear Regression, **(b)** Random Forest, and **(c)** Convolutional Neural Network. **(d)** Canopy Height Density plot of LiDAR derived canopy height at 10 m resolution for comparison. NB: To aid visualisation **(a)** is missing 74 rows of data, as they are not within the fixed axis limits.

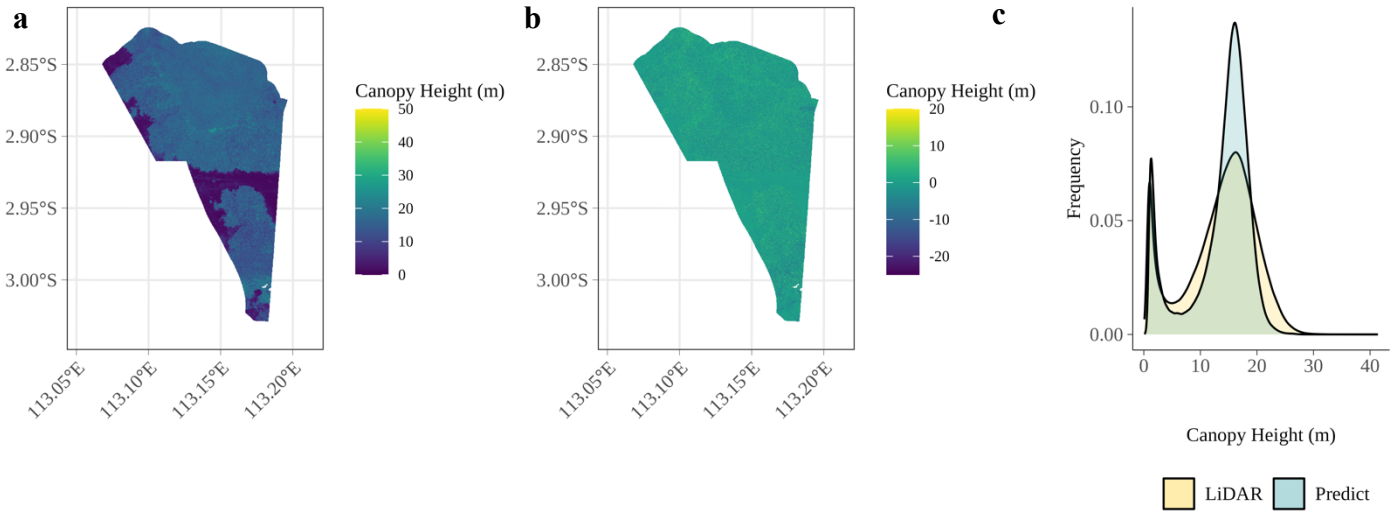

Figure 18. **(a)** Predicted Canopy Height Model from the Convolutional Neural Network for the Sentinel-2 at 10 m resolution data **(b)** Difference between the Predicted Canopy Height and the LiDAR derived Canopy Height. **(c)** density plot comparing the canopy height derived from LiDAR and the predicted canopy height (m).

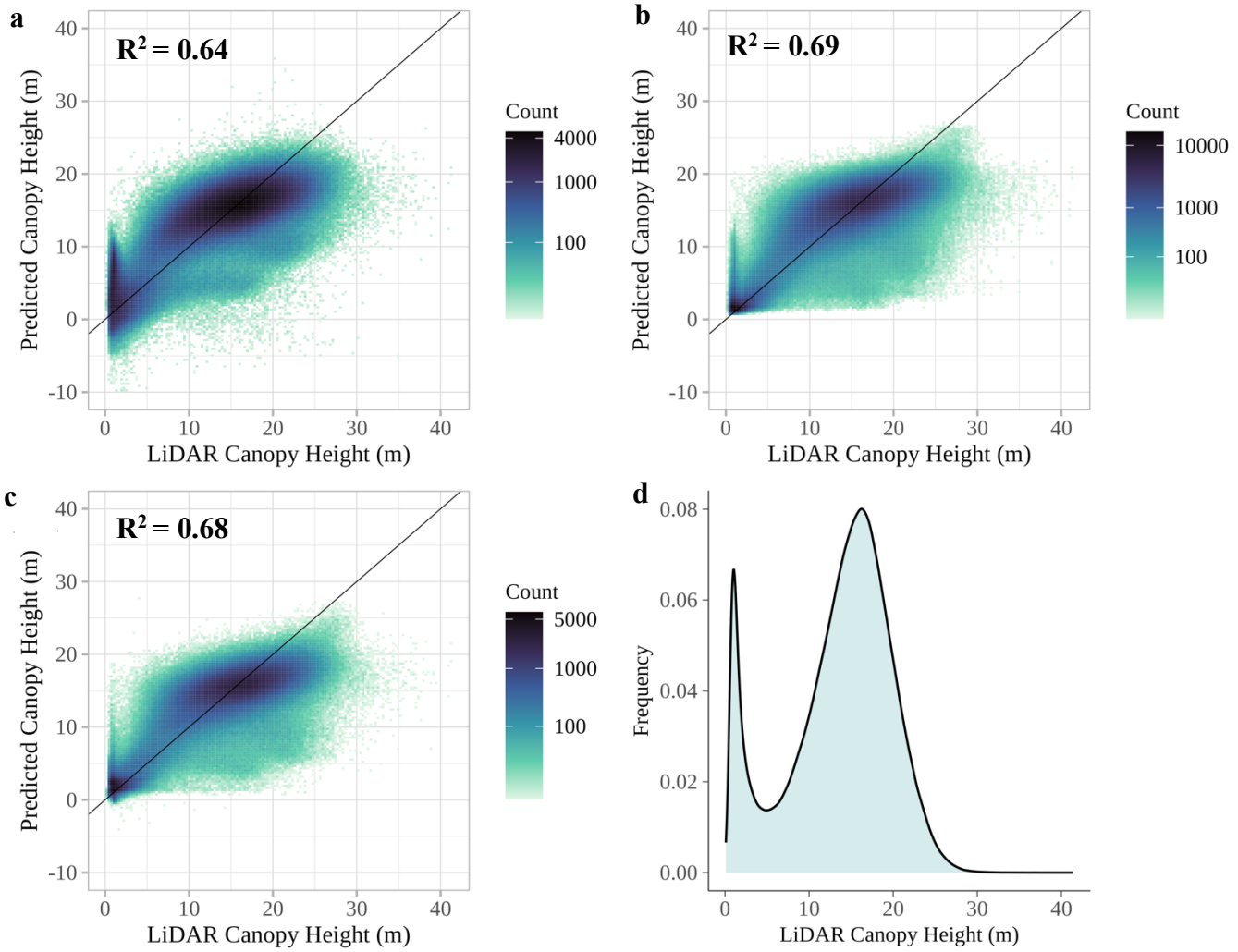

Figure 19. Scatterplots of predicted canopy height (m) for the Combined Data Source of PlanetScope and Sentinel-2 at 10 m resolution using **(a)** Multiple Linear Regression, **(b)** Random Forest, and **(c)** Convolutional Neural Network. **(d)** Canopy Height Density plot of LiDAR derived canopy height at 10 m resolution for comparison. NB: To aid visualisation **(a)** is missing 74 rows of data, as they are not within the fixed within the y axis limits.

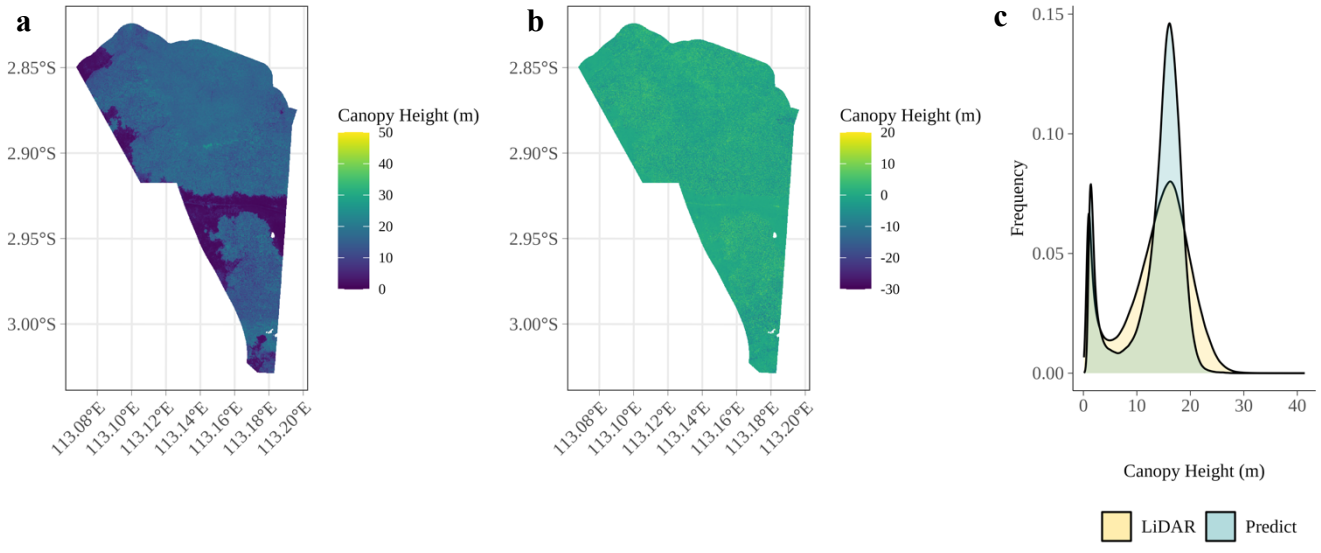

Figure 20. (a) Predicted Canopy Height Model from the Combined Data Source of PlanetScope and Sentinel-2 at 10 m resolution data **(b)** Difference between the Predicted Canopy Height and the LiDAR derived Canopy Height. **(c)** density plot comparing the canopy height derived from LiDAR and the predicted canopy height (m).

4. Discussion

Several studies have demonstrated the efficacy of utilising airborne LiDAR data for the generation of canopy height models. However, due to the high cost associated with the acquisition of airborne LiDAR data, other approaches have been embraced to upscale these canopy height models. This includes using optical satellite imagery and machine learning algorithms. In this study, optical data from both Sentinel-2 and PlanetScope were compared to test their ability to predict canopy height derived from LiDAR within the Katingan Mentaya Project, Central Kalimantan. This included PlanetScope at 3 and 10 m resolution, Sentinel-2 at 10 m resolution, and a combination of PlanetScope and Sentinel-2 at 10 m resolution. Further to this, three machine learning algorithms (multiple linear regression, random forest, and convolutional neural network) were compared, to see how the predictive accuracy varied as well as investigating their reproducibility to be used within industry.

In all cases the non-parametric models (random forest and convolutional neural network) outperformed the parametric model of multiple linear regression, however, the MLR was the fastest running model, where feature selection by "find_correlation", cross-validation by repeated coordinated-based k-means clustering, and training took between 3.82 minutes (Sentinel -2) and 34.41 minutes (PlanetScope 3 m). Although studies have not directly compared multiple linear regression models with convolutional neural networks, some studies have compared the performance of RF with MLR and RF with a CNN. Those that have completed RF with MLR, have documented the RF outperforming the MLR. Dube et al. (2015) examined the ability of multi-source data consisting of SPOT-5 raw spectral features (four bands), 14 spectral vegetation indices, rainfall data, and stand to predict both stand volume and eucalyptus tree height in Zululand, South Africa, at 10 m resolution. In all cases the RF outperformed the MLR. The RF model had an R^2 and RMSE of 0.46 and 2.84 m compared to the MLR of 0.4, and 3.05 m, respectively. The increase in accuracy when using random forest to predict canopy height is due to the elements of stochasticity that are responsible for improving model accuracy and reducing model overfitting (Dube et al., 2015).

Torres de Almeida et al. (2022) also compared the performances of RF and MLR as well as Classification and Regression Trees (CART) when using Sentinel-1 and Sentinel-2 data with a multisensory approach for modelling canopy height in the Atlantic Forest of Paraná, Brazil. This included comparing models across different dates, spatial resolutions and including different features from the reflectance bands (raw), the vegetation indices (ind) and the complete feature set of reflectance and vegetation indices (all). Overall, Torres de Almeida et al. (2022) found that RF was the highest performing model across all models. When comparing Sentinel-2 at 10 m x 10 m resolution, the models of RF and MLR performance were very similar, however, the MLR had a slightly higher R^2 of 0.38 from the date of October 26 with all features, compared to the highest performing RF on November 30 with all features with an R^2 of 0.35. However, the RF overall had a

lower RMSE ranging from 6.76 m to 8.31 m compared to the MLR which ranged from 6.68 m to 10.37 m. This is similar to this current study, where in all cases the RF had a lower RMSE ranging from 3.47 m to 5.50 m, compared to the MLR which had an RMSE ranging from 3.70 m to 5.76 m.

When comparing Random Forest with Convolutional Neural Networks, all data sources had a very similar performance across MAE, RMSE and R^2. However, the CNN took longer for all data sources, especially at PlanetScope 3 m resolution, where the CNN took 6 times longer than the RF model at 2723 minutes. Shah et al. (2020) also compared the ability of CNNs to estimate canopy height against RF using Landsat at 30 m resolution in Flagstaff, Arizona. The comparison included investigating the performance of a CNN with all features, a CNN with features selected from RF as outlined in Staben et al. (2018), a Random Forest regression model, and finally a CNN with features selected from their own CNN-based approach. The RF regression model had a lower mean absolute error of 2.33 m and mean square error (MSE) of 0.686 m compared to a CNN with all features (MAE = 3.65 m, MSE = 1.05 m), CNN with features selected from an RF model from Staben et al. (2018) (MAE = 3.43 m and MSE = 0.98 m), and CNN with features selected from their own CNN based feature selection (MAE = 3.092 m and MSE = 0.8872 m). However, the RF regression model had a high variance of 5.17 m compared to the other CNN models which ranged from 0.864 m to 1.009 m. This high variance is due to the fact they used the features selected from the Random Forest modelling from the study by Staben et al. (2018) which was completed in a completely different geographic region in Darwin, Australia and not from their own geographical location. This demonstrates that the importance of features varies from location to location, and also shows that a Random Forest model of importance features may not be able to simply be applied to a different location. Further to this, the study completed by Shah et al. (2020) demonstrates a potential limitation in this current study, where the CNN model was only developed based on all features. As Shah et al. (2020) show, the CNN with all features produced the lowest performance of all their models. There is potential for the CNN models developed in this current study to improve in performance if feature selection is applied. Further studies could investigate how RF feature selection applied to the same geographical location is fed into CNN compared to a CNN with all features, an RF with the features selected from the RF, and a CNN that has selected features from its own CNN features selection. However, in terms of reproducibility, this may not be best suited to industry due to the computational time, especially in terms of creating feature selection through a CNN, as this requires feeding each feature individually through a simple CNN base model and then ranking them based on the least mean square validation score. Overall, although other studies have highlighted the potential of using a CNN in predicting canopy height due to its ability to use the spatial association of neighbouring pixels for classification, the CNN in this study did not outperform the RF, and this may be due to the high degree of spatial autocorrelation within the study site, where neighbouring pixels would be quite similar to one another, and therefore may not offer any extra information. Overall, this study has demonstrated that an RF which includes feature selection, can perform as well as the CNN, and significantly cut down on

computational time. However, further exploration is needed on how feature selection varies between geographical locations, and whether the features of this location can also be applied to other tropical forest regions.

The current machine learning algorithms have been developed in an area that has relatively flat terrain and only contains information from one particular season. As demonstrated by Shah et al. (2020), feature selection may not directly apply from location to location, and therefore these current models may not be able to be directly applied to other geographical regions and different time periods. Future work should investigate the integration of multi-seasonal data for the prediction of canopy height. Shimizu et al. (2020) found that the integration of multi-seasonal composite images offers advantages over time-series or a single-composite image in predicting canopy height, such as capturing seasonal variations and vegetation phenology. The multi-seasonal composite images have the ability to capture temporal variability, reducing biases associated with a singular season. Incorporating images over multiple seasons can provide a more comprehensive view of canopy characteristics and facilitate the identification of both short-term fluctuations and long-term trends.

Another possibility to create canopy height models that can be used across different geographical regions is to investigate the potential of using spaceborne LiDAR for calibration of canopy height, rather than airborne LiDAR, with missions such as NASA's Global Ecosystem Dynamic Investigation (GEDI) (Adrah et al., 2022; Fayad et al., 2021; Gupta and Sharma, 2022; Lang et al., 2022b) or the Geoscience Laser Altimeter System (GLAS) aboard ICESat (Ice, Cloud, and land Elevation Satellite) (Hudak et al., 2002; Khalefa et al., 2013). Calibration through spaceborne LiDAR technology presents a range of advantages including global coverage (Lang et al., 2022b), consistent data acquisition, accessibility, and temporal analysis (Coops et al., 2021; Dhargay et al., 2022). The global coverage of spaceborne LiDAR not only facilitates large-scale ecological and environmental studies, but also ensures data consistency and reproducibility over time. Unlike airborne surveys, which can exhibit variations due to diverse flight paths and sensor setups, spaceborne LiDAR missions offer standardized data collection that enables robust cross-site comparisons and temporal analyses (Coops et al., 2021). These advantages demonstrate spaceborne LiDAR as a valuable tool for understanding canopy dynamics, ecosystem health, and environmental changes on a global scale. However, the spatial and temporal resolution of spaceborne airborne LiDAR is limited to that of airborne LiDAR, therefore it would be interesting to compare the predictive accuracy of canopy height of the models developed in this study when calibrated with airborne LiDAR versus spaceborne LiDAR.

All machine learning algorithms and data sources were able to differentiate between forest and non-forest areas, however, due to the dense and complex canopy cover across the forested areas, there were consistent inaccuracies in canopy height predictions in these areas (Figure 13 – 20). The difficulty in detecting the differences in canopy height could be attributed to the fact that dense

canopies often consist of intricate structures of overlapping branches, leaves, and stems, which can lead to complex light interactions that are difficult to interpret. Further to this, all machine learning algorithms demonstrated an underestimation of canopy heights when predicting beyond 20 m. This has also been seen in other studies that have incorporated optical satellite data to predict canopy height (Hansen et al., 2016; Shimizu et al., 2020). This could be due to two reasons, including that few data points were beyond 20 m, where the majority of the canopy heights were between 0 to 5 m and 10 to 20 m (Figure 4), meaning that the machine learning algorithms may not have had enough data points for these areas to effectively learn the characteristics of these heights. This underestimation could also be explained by saturation of reflectance at certain heights, and shadows cast by taller vegetation can also lead to variations in light intensity, making it difficult to distinguish between canopy elements (Shimizu et al., 2020). To overcome these limitations, alternative data sources and sensing techniques such as synthetic aperture radar (SAR) may be used, which may provide more reliable measurements of vertical structures. SAR has the ability to observe forest structure even in cloudy conditions (Bae et al., 2019). Further to this, SAR can effectively penetrate forest canopy using its signal, allowing for the retrieval of additional information regarding the canopy's structure and density (Xi et al., 2022). A study completed by Gupta and Sharma (2022) used features extracted from multispectral optical data (Landsat-8 and Sentinel-2), along with SAR (ALOS-2/PALSAR-2, Sentinel-1), and found that the ALOS-2/ PALSAR-2 backscatters HV (Horizontal-Vertical) and HH (Horizontal-Horizontal) were within the top five predictors of predicting canopy height, as they are the most sensitive to vegetation structures and show the highest sensitivity to biomass (Bindlish and Barros, 2001). Therefore, future studies could investigate the integration of optical and SAR satellite data, such as ALOS-2 and PALSAR-2 for estimating canopy height in tropical forests.

PlanetScope at 3 m resolution was the lowest performing model across all machine learning algorithms and compared to the other data sources. In all cases, the accuracy of the model was below 0.5. This demonstrates that although this data compliments Sentinel-2 with finer spatial resolution and temporal coverage, it does not improve the prediction of canopy height. Although it has been shown that the fine spatial resolution from PlanetScope can be beneficial for certain applications like land cover classification and mapping (Acharki, 2022; Rösch et al., 2022), as canopy height is a vertical measurement, the finer spatial resolution does not necessarily provide more information about the vertical structure of the vegetation. A study completed by Shimizu (2020) also investigated the potential of PlanetScope 3 m resolution using random forest within a temperate forest and this produced an R^2 of 0.62, however, the distribution of tree canopy height ranged from 0 to 25 m, and similarly the 3 m resolution had difficulty predicting the higher range of trees, where it rarely predicted beyond ~ 14 m. This is compared to our current study, where the tree canopy height ranged from 0 to 47 m at 3 m resolution. This demonstrates that the use of PlanetScope data may best be suited to areas that have a lower canopy height. Further to this, when Shimizu et al. (2020) increased

the PlanetScope data to 10 m resolution it did increase the R^2 to 0.69, but again, rarely predicted beyond 15 m (Shimizu et al., 2020). The higher R^2 score obtained by PlanetScope data could also be attributed to the inclusion of texture measures in the Shimizu et al. (2020) study, where they included seven first and second-order texture measures that were calculated as grey-level co-occurrence matrix (GLCM). The inclusion of textural variables are good indicators of vegetation structure as well as spatial characteristics of tree canopies (Wood et al., 2012). However, as outlined in Shimizu et al. (2020) and Csillik et al. (2020) the role of textural information derived from the PlanetScope data is not evident and requires additional exploration. The study by Shimizu et al. (2020) also demonstrated an increase in performance compared to PlanetScope data when using Sentinel-2 data at 10 m resolution, where the R^2 increased from 0.69 to 0.73, which is also seen in this study, where the PlanetScope at 10 m resolution had an R^2 of 0.60 compared to Sentinel-2 which obtained the highest R^2 of 0.69.

The increase in performance from PlanetScope to Sentinel-2 demonstrates that the extra spectral bands within Sentinel-2 provided a more comprehensive analysis of vegetation properties to help inform canopy estimation. This is evident within the feature selection of the combined model, where 36 different features were inputted into the model, and the top 5 features came from the Sentinel-2 band. Further to this, when comparing Sentinel-2 to the combined dataset, it demonstrated a very similar performance, revealing the addition of PlanetScope spectral bands does not have a significant contribution to forest structural estimates in tropical forests. This is also supported by a study completed by Mulatu et al. (2019), where the PlanetScope-derived vegetation indices, did not have a significant contribution to the prediction of forest structural elements. The red-edge band from Sentinel-2 and the extra band of SWIR 1 (BAND 11, named SWIR_11 in the feature importance chart) demonstrate to be of high importance in predicting canopy height, which is also supported by other studies (Astola et al., 2019; Li et al., 2020; Mulatu et al., 2019; Shimizu et al., 2020). In this study, the red-edge band was always within the first two features and the SWIR 1 band was within the top 10 features (Figure 8 – 11). The shortwave infrared band has been reported as an important feature for predicting canopy height and aboveground biomass due to its ability to provide a good contrast between different types of vegetation and is useful in measuring the moisture content of soil (Dube et al., 2015; Main-Knorn et al., 2013; Sentinel-Hub, 2023b). As the SWIR 1 provides information on moisture content of soil and this is closely related to water availability, trees with access to adequate water resources are more likely to have healthier and taller canopies.

As mentioned, the PlanetScope data at 3 m resolution is freely available due to Norway's International Climate and Forest Initiative, however, if this study were to be repeated outside of the tropics, it is not guaranteed that special permission can be given for free download. As seen in this study, combining PlanetScope with Sentinel-2 does not dramatically improve the performance of canopy height predictions, and in some cases Sentinel-2 on its own performs better. Therefore, it is

recommended that Sentinel-2 along with the non-parametric model of Random Forest is the most effective model for predicting canopy height. The next step would be to use the information generated from the canopy height model to determine above ground biomass. Unlike other LiDAR-based measurements, with complex nonlinear relationships with above-ground biomass, the correlation between canopy height and above-ground biomass is linear (Meyer et al., 2018). By determining the above ground biomass in tropical forests, valuable information can be provided for forest monitoring, management, planning, and assessing, which aligns with REDD+ initiatives.

5. Conclusion

Through this study, it is evident that open-source remote sensing data, combined with machine learning can be a powerful tool in mapping canopy height in tropical forests. This study provides valuable insights regarding the most appropriate data source and machine learning algorithm for predicting canopy height in tropical forests. Although other studies have demonstrated CNNs ability to create accurate canopy height models, their reproducibility is constrained by the large data volume and computational resource required for effective implementation. Therefore, it is recommended that RF is used when predicting canopy height. However, further exploration is needed to determine whether the features selected from the Sentinel-2 at 10 m resolution can also be applied to other tropical forest regions. Further to this, the addition of PlanetScope data did not drastically improve canopy height predictions, and because PlanetScope data is not always freely available, it is recommended that Sentinel-2 data along with RF is used to improve assessment of canopy height predictions in tropical forests. Overall, the insight within this study contributes to the field of remote sensing and ecological analyses, offering valuable guidance for predicting canopy height in tropical forest regions, which is crucial for carbon storage estimation and understanding forest structure.

Appendix

Appendix 1: Data Availability Statement

The code to train and develop the various machine learning algorithms is available at: https://github.com/TESS-Laboratory/Pickstone-development

Appendix 2: Note on Data Size

- PlanetScope 3 m data table: 17,405,911 rows x 29 columns
- PlanetScope 10 m data table: 1,566,545 x 29 columns
- Sentinel-2 data table: 1,564,685 rows x 32 columns
- Combined data table: 1,563,954 rows x 53 columns

NB: the difference in rows between PlanetScope 10m, Sentinel-2 and Combined data is due to the cloud and shadow masking.

Appendix 3: Performance of Models

Table A3.1. Comparison of the performance and time of Random Forest model of 300,000 pixels and 20% of the data

Data Source	**RF (300,000 pixels)**				**RF (5 %)**			
	MAE	RMSE	R^2	Time (mins)	MAE	RMSE	R^2	Time (mins)
PlanetScope (3 m)	4.26	5.49	0.425	610.98	4.27	5.50	0.423	450.35
PlanetScope (10 m)	2.99	3.94	0.60	830.23	3.01	3.97	0.60	31.48
Sentinel-2 (10 m)	2.59	3.47	0.687	223.45	2.63	3.52	0.684	34.23
Planet Scope and Sentinel-2 (10m)	2.54	3.43	0.695	245.65	2.58	3.47	0.689	33.53

A range of subsample of 5 – 20% of the data was tested, and all yielded quite similar results to the above comparison for PlanetScope 10 m, Sentinel-2 10 m and the combined dataset. However, when using 10% and above of PlanetScope 3 m, over 600 GB of RAM was required. This meant that it would usually crash and terminate R after 16+ hours of running. This is why 5% was chosen, as it had a faster completion time, and still yielded similar results.

Table A3.2. Hyperparameter tuning results of Random Forest models from different data sources

	PlanetScope 3 m	**PlanetScope 10 m**	**Sentinel-2**	**Combined**
Importance Filter Fraction	0.56	0.79	0.52	0.69
mtry	4	5	4	8
Sample Fraction	0.59	0.77	0.69	0.997
Minimum Node Size	5	1	1	3
Replace	True	True	False	True

Table A3.3. Performance metrics of each machine learning algorithm, using PlanetScope and Sentinel-2 data for prediction of canopy height

Data Source	**MLR**				**RF**				**CNN**			
	MAE	RMSE	R^2	Time (mins)	MAE	RMSE	R^2	Time (mins)	MAE	RMSE	R^2	Time (mins)
PlanetScope (3 m)	4.61	5.76	0.37	34.41	4.27	5.50	0.43	450.35	4.32	5.53	0.42	2723.23
PlanetScope (10 m)	3.48	4.40	0.50	3.99	3.01	3.97	0.60	31.48	3.05	3.95	0.60	126.86
Sentinel-2 (10 m)	2.89	3.70	0.65	3.82	2.63	3.52	0.68	34.23	2.64	3.47	0.69	77.35
Planet Scope and Sentinel-2 (10m)	2.90	3.73	0.64	5.25	2.58	3.47	0.69	33.53	2.68	3.50	0.68	155.65

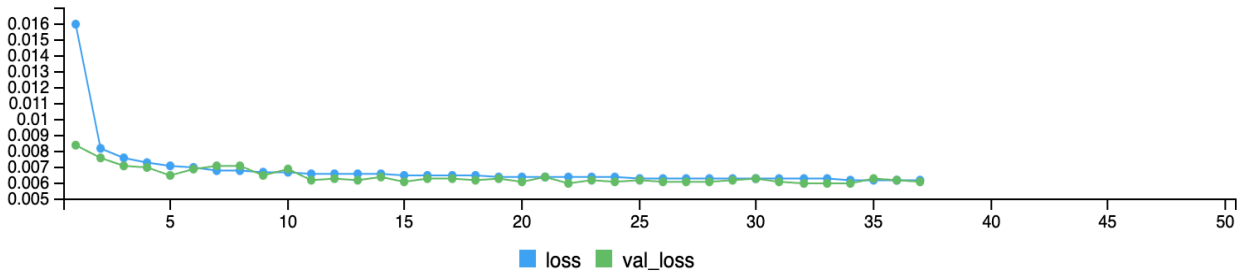

Figure A3.1. Training and validation loss curves for the Sentinel-2 10 m x 10 m resolution. This demonstrates the early stopping call back where the training was stopped after 37 epochs

References

Acharki, S., 2022. PlanetScope contributions compared to Sentinel-2, and Landsat-8 for LULC mapping. Remote Sens. Appl. Soc. Environ. 27, 100774. https://doi.org/10.1016/j.rsase.2022.100774

Adrah, E., Wan Mohd Jaafar, W.S., Omar, H., Bajaj, S., Leite, R.V., Mazlan, S.M., Silva, C.A., Chel Gee Ooi, M., Mohd Said, M.N., Abdul Maulud, K.N., Cardil, A., Mohan, M., 2022. Analyzing Canopy Height Patterns and Environmental Landscape Drivers in Tropical Forests Using NASA's GEDI Spaceborne LiDAR. Remote Sens. 14, 3172. https://doi.org/10.3390/rs14133172

Ahmed, O.S., Franklin, S.E., Wulder, M.A., White, J.C., 2015. Characterizing stand-level forest canopy cover and height using Landsat time series, samples of airborne LiDAR, and the Random Forest algorithm. ISPRS J. Photogramm. Remote Sens. 101, 89–101. https://doi.org/10.1016/j.isprsjprs.2014.11.007

Anderson, J., Plourde, L., Martin, M., Braswell, B., Smith, M., Dubayah, R., Hofton, M., Blair, J., 2008. Integrating waveform lidar with hyperspectral imagery for inventory of a northern temperate forest. Remote Sens. Environ. 112, 1856–1870. https://doi.org/10.1016/j.rse.2007.09.009

Anderson, M., Neale, C., Li, F., Norman, J., Kustas, W., Jayanthi, H., Chavez, J., 2004. Upscaling ground observations of vegetation water content, canopy height, and leaf area index during SMEX02 using aircraft and Landsat imagery. Remote Sens. Environ. 92, 447–464. https://doi.org/10.1016/j.rse.2004.03.019

Appel, M., Pebesma, E., Mohr, M., 2021. Cloud-based processing of satellite image collections in R using STAC, COGs, and on-demand data cubes.

Astola, H., Häme, T., Sirro, L., Molinier, M., Kilpi, J., 2019. Comparison of Sentinel-2 and Landsat 8 imagery for forest variable prediction in boreal region. Remote Sens. Environ. 223, 257–273. https://doi.org/10.1016/j.rse.2019.01.019

Bae, S., Levick, S.R., Heidrich, L., Magdon, P., Leutner, B.F., Wöllauer, S., Serebryanyk, A., Nauss, T., Krzystek, P., Gossner, M.M., Schall, P., Heibl, C., Bässler, C., Doerfler, I., Schulze, E.-D., Krah, F.-S., Culmsee, H., Jung, K., Heurich, M., Fischer, M., Seibold, S., Thorn, S., Gerlach, T., Hothorn, T., Weisser, W.W., Müller, J., 2019. Radar vision in the mapping of forest biodiversity from space. Nat. Commun. 10, 4757. https://doi.org/10.1038/s41467-019-12737-x

Bayrak, M., Marafa, L., 2016. Ten Years of REDD+: A Critical Review of the Impact of REDD+ on Forest-Dependent Communities. Sustainability 8, 620. https://doi.org/10.3390/su8070620

Bendig, J., Yu, K., Aasen, H., Bolten, A., Bennertz, S., Broscheit, J., Gnyp, M.L., Bareth, G., 2015. Combining UAV-based plant height from crop surface models, visible, and near infrared vegetation indices for biomass monitoring in barley. Int. J. Appl. Earth Obs. Geoinformation 39, 79–87. https://doi.org/10.1016/j.jag.2015.02.012

Bergstra, J., Bengio, Y., 2012. Random Search for Hyper-Parameter Optimization. J. Mach. Learn. Res. 13, 281–305.

Berrar, D., 2019. Cross-Validation, in: Encyclopedia of Bioinformatics and Computational Biology. Elsevier, pp. 542–545. https://doi.org/10.1016/B978-0-12-809633-8.20349-X

Bindlish, R., Barros, A.P., 2001. Parameterization of vegetation backscatter in radar-based, soil moisture estimation. Remote Sens. Environ. 76, 130–137. https://doi.org/10.1016/S0034-4257(00)00200-5

Bohling, G., 2005. Introduction to geostatistics and variogram analysis. Kans. Geol. Surv. 1, 1--20.

Brandon, K., 2014. Ecosystem Services from Tropical Forests: Review of Current Science. SSRN Electron. J. https://doi.org/10.2139/ssrn.2622749

Breiman, L., 2001. Random Forests. Mach. Learn. 45, 5–32. https://doi.org/10.1023/A:1010933404324

Brenning, A., 2012. Spatial cross-validation and bootstrap for the assessment of prediction rules in remote sensing: The R package sperrorest, in: 2012 IEEE International Geoscience and Remote Sensing Symposium. Presented at the IGARSS 2012 - 2012 IEEE International Geoscience and Remote Sensing Symposium, IEEE, Munich, Germany, pp. 5372–5375. https://doi.org/10.1109/IGARSS.2012.6352393

Brodrick, P.G., Davies, A.B., Asner, G.P., 2019. Uncovering Ecological Patterns with Convolutional Neural Networks. Trends Ecol. Evol. 34, 734–745. https://doi.org/10.1016/j.tree.2019.03.006

Caughlin, T.T., Rifai, S.W., Graves, S.J., Asner, G.P., Bohlman, S.A., 2016. Integrating Li DAR - derived tree height and Landsat satellite reflectance to estimate forest regrowth in a tropical agricultural landscape. Remote Sens. Ecol. Conserv. 2, 190–203. https://doi.org/10.1002/rse2.33

Chollet, F., Allaire, J., 2017. R Interface to Keras.

Congalton, R.G., 1988. Using Spatial Autocorrelation Analysis to Explore the Errors in Maps Generated from Remotely Sensed Data. Photogramm. Eng. Remote Sens. 54, 587–592.

Constantino, K.P., Gonzales, E.J., Lazaro, L.M., Serrano, E.C., Samson, B.P., 2018. Towards an Automated Plant Height Measurement and Tiller Segmentation of Rice Crops using Image Processing, in: Billingsley, J., Brett, P. (Eds.), Mechatronics and Machine Vision in Practice 3. Springer International Publishing, Cham, pp. 155–168. https://doi.org/10.1007/978-3-319-76947-9_11

Coops, N.C., Tompalski, P., Goodbody, T.R.H., Queinnec, M., Luther, J.E., Bolton, D.K., White, J.C., Wulder, M.A., Van Lier, O.R., Hermosilla, T., 2021. Modelling lidar-derived estimates of forest attributes over space and time: A review of approaches and future trends. Remote Sens. Environ. 260, 112477. https://doi.org/10.1016/j.rse.2021.112477

Corbera, E., Schroeder, H., 2011. Governing and implementing REDD+. Environ. Sci. Policy 14, 89–99. https://doi.org/10.1016/j.envsci.2010.11.002

Csillik, O., Kumar, P., Asner, G.P., 2020. Challenges in Estimating Tropical Forest Canopy Height from Planet Dove Imagery. Remote Sens. 12, 1160. https://doi.org/10.3390/rs12071160

Cunliffe, A.M., Anderson, K., Boschetti, F., Brazier, R.E., Graham, H.A., Myers-Smith, I.H., Astor, T., Boer, M.M., Calvo, L.G., Clark, P.E., Cramer, M.D., Encinas-Lara, M.S., Escarzaga, S.M., Fernández-Guisuraga, J.M., Fisher, A.G., Gdulová, K., Gillespie, B.M., Griebel, A., Hanan, N.P., Hanggito, M.S., Haselberger, S., Havrilla, C.A., Heilman, P., Ji, W., Karl, J.W., Kirchhoff, M., Kraushaar, S., Lyons, M.B., Marzolff, I., Mauritz, M.E., McIntire, C.D., Metzen, D., Méndez-Barroso, L.A., Power, S.C., Prošek, J., Sanz-Ablanedo, E., Sauer, K.J., Schulze-Brüninghoff, D., Šímová, P., Sitch, S., Smit, J.L., Steele, C.M., Suárez-Seoane, S., Vargas, S.A., Villarreal, M., Visser, F., Wachendorf, M., Wirnsberger, H., Wojcikiewicz, R., 2022. Global application of an unoccupied aerial vehicle photogrammetry protocol for predicting aboveground biomass in non-forest ecosystems. Remote Sens. Ecol. Conserv. 8, 57–71. https://doi.org/10.1002/rse2.228

Cunliffe, A.M., McIntire, C.D., Boschetti, F., Sauer, K.J., Litvak, M., Anderson, K., Brazier, R.E., 2020. Allometric relationships for predicting aboveground biomass and sapwood area of Oneseed Juniper (Juniperus monosperma) trees. Front. Plant Sci. 11, 1–12. https://doi.org/10.3389/fpls.2020.00094

Dhargay, S., Lyell, C.S., Brown, T.P., Inbar, A., Sheridan, G.J., Lane, P.N.J., 2022. Performance of GEDI Space-Borne LiDAR for Quantifying Structural Variation in the Temperate Forests of South-Eastern Australia. Remote Sens. 14, 3615. https://doi.org/10.3390/rs14153615

Ding, Z., Li, R., O'Connor, P., Zheng, H., Huang, B., Kong, L., Xiao, Y., Xu, W., Ouyang, Z., 2021. An improved quality assessment framework to better inform large-scale forest restoration management. Ecol. Indic. 123, 107370. https://doi.org/10.1016/j.ecolind.2021.107370

Ditt, E.H., Mourato, S., Ghazoul, J., Knight, J., 2010. Forest conversion and provision of ecosystem services in the Brazilian Atlantic Forest. Land Degrad. Dev. 21, 591–603. https://doi.org/10.1002/ldr.1010

Dubayah, R.O., Sheldon, S.L., Clark, D.B., Hofton, M.A., Blair, J.B., Hurtt, G.C., Chazdon, R.L., 2010. Estimation of tropical forest height and biomass dynamics using lidar remote sensing at La Selva, Costa Rica. J. Geophys. Res. Biogeosciences 115. https://doi.org/10.1029/2009JG000933

Dube, T., Mutanga, O., Abdel-Rahman, E.M., Ismail, R., Slotow, R., 2015. Predicting Eucalyptus spp. stand volume in Zululand, South Africa: an analysis using a stochastic gradient boosting regression ensemble with multi-source data sets. Int. J. Remote Sens. 36, 3751–3772. https://doi.org/10.1080/01431161.2015.1070316

ElGharbawi, T., Susaki, J., Chureesampant, K., Arunplod, C., Thanyapraneedkul, J., Limlahapun, P., Suliman, A., 2023. Performance evaluation of convolution neural networks in canopy height estimation using sentinel 2 data, application to Thailand. Int. J. Remote Sens. 44, 1726–1748. https://doi.org/10.1080/01431161.2023.2189035

European Space Agency, 2023a. ESA - Sentinel-2 [WWW Document]. Eur. Space Agency. URL https://www.esa.int/Applications/Observing_the_Earth/Copernicus/Sentinel-2 (accessed 5.26.23).
European Space Agency, 2023b. Copernicus Digital Elevation Model [WWW Document]. Copernic. Contrib. Missions Online. URL https://spacedata.copernicus.eu/collections/copernicus-digital-elevation-model (accessed 7.28.23).
Fassnacht, F.E., Poblete-Olivares, J., Rivero, L., Lopatin, J., Ceballos-Comisso, A., Galleguillos, M., 2021. Using Sentinel-2 and canopy height models to derive a landscape-level biomass map covering multiple vegetation types. Int. J. Appl. Earth Obs. Geoinformation 94, 102236. https://doi.org/10.1016/j.jag.2020.102236
Fayad, I., Ienco, D., Baghdadi, N., Gaetano, R., Alvares, C.A., Stape, J.L., Ferraço Scolforo, H., Le Maire, G., 2021. A CNN-based approach for the estimation of canopy heights and wood volume from GEDI waveforms. Remote Sens. Environ. 265, 112652. https://doi.org/10.1016/j.rse.2021.112652
García, M., Saatchi, S., Ustin, S., Balzter, H., 2018. Modelling forest canopy height by integrating airborne LiDAR samples with satellite Radar and multispectral imagery. Int. J. Appl. Earth Obs. Geoinformation 66, 159–173. https://doi.org/10.1016/j.jag.2017.11.017
Gardner, T.A., Barlow, J., Chazdon, R., Ewers, R.M., Harvey, C.A., Peres, C.A., Sodhi, N.S., 2009. Prospects for tropical forest biodiversity in a human-modified world. Ecol. Lett. 12, 561–582. https://doi.org/10.1111/j.1461-0248.2009.01294.x
Ghosh, S.M., Behera, M.D., Paramanik, S., 2020. Canopy Height Estimation Using Sentinel Series Images through Machine Learning Models in a Mangrove Forest. Remote Sens. 12, 1519. https://doi.org/10.3390/rs12091519
Gitelson, A., Merzlyak, M.N., 1994. Quantitative estimation of chlorophyll-a using reflectance spectra: Experiments with autumn chestnut and maple leaves. J. Photochem. Photobiol. B 22, 247–252. https://doi.org/10.1016/1011-1344(93)06963-4
Gitelson, A.A., Gritz †, Y., Merzlyak, M.N., 2003. Relationships between leaf chlorophyll content and spectral reflectance and algorithms for non-destructive chlorophyll assessment in higher plant leaves. J. Plant Physiol. 160, 271–282. https://doi.org/10.1078/0176-1617-00887
Gitelson, A.A., Kaufman, Y.J., Merzlyak, M.N., 1996. Use of a green channel in remote sensing of global vegetation from EOS-MODIS. Remote Sens. Environ. 58, 289–298. https://doi.org/10.1016/S0034-4257(96)00072-7
Gupta, R., Sharma, L.K., 2023. Mapping Canopy Height from ICESat-2 and Landsat-9 using Machine Learning in the Himalayan Corbett Tiger Reserve, India, in: 2023 International Conference on Machine Intelligence for GeoAnalytics and Remote Sensing (MIGARS). Presented at the 2023 International Conference on Machine Intelligence for GeoAnalytics and Remote Sensing (MIGARS), pp. 1–4. https://doi.org/10.1109/MIGARS57353.2023.10064540
Gupta, R., Sharma, L.K., 2022. Mixed tropical forests canopy height mapping from spaceborne LiDAR GEDI and multisensor imagery using machine learning models. Remote Sens. Appl. Soc. Environ. 27, 100817. https://doi.org/10.1016/j.rsase.2022.100817
Hansen, M.C., Potapov, P.V., Goetz, S.J., Turubanova, S., Tyukavina, A., Krylov, A., Kommareddy, A., Egorov, A., 2016. Mapping tree height distributions in Sub-Saharan Africa using Landsat 7 and 8 data. Remote Sens. Environ. 185, 221–232. https://doi.org/10.1016/j.rse.2016.02.023
Hijmans, R.J., 2023. terra: Spatial Data Analysis.
Hudak, A.T., Crookston, N.L., Evans, J.S., Hall, D.E., Falkowski, M.J., 2008. Nearest neighbor imputation of species-level, plot-scale forest structure attributes from LiDAR data. Remote Sens. Environ. 112, 2232–2245. https://doi.org/10.1016/j.rse.2007.10.009
Hudak, A.T., Lefsky, M.A., Cohen, W.B., Berterretche, M., 2002. Integration of lidar and Landsat ETM+ data for estimating and mapping forest canopy height. Remote Sens. Environ. 82, 397–416. https://doi.org/10.1016/S0034-4257(02)00056-1
Huete, A., 1997. A comparison of vegetation indices over a global set of TM images for EOS-MODIS. Remote Sens. Environ. 59, 440–451. https://doi.org/10.1016/S0034-4257(96)00112-5
IETA, 2018. The Katingan Mentaya Project.
Isaaks, E.H., Srivastava, R.M., 1989. Applied geostatistics. Oxford University Press.
Jucker, T., Caspersen, J., Chave, J., Antin, C., Barbier, N., Bongers, F., Dalponte, M., Van Ewijk, K.Y., Forrester, D.I., Haeni, M., Higgins, S.I., Holdaway, R.J., Iida, Y., Lorimer, C., Marshall, P.L., Momo, S., Moncrieff, G.R., Ploton, P., Poorter, L., Rahman, K.A., Schlund, M., Sonké, B.,

Sterck, F.J., Trugman, A.T., Usoltsev, V.A., Vanderwel, M.C., Waldner, P., Wedeux, B.M.M., Wirth, C., Wöll, H., Woods, M., Xiang, W., Zimmermann, N.E., Coomes, D.A., 2017. Allometric equations for integrating remote sensing imagery into forest monitoring programmes. Glob. Change Biol. 23, 177–190. https://doi.org/10.1111/gcb.13388

Kacic, P., Kuenzer, C., 2022. Forest Biodiversity Monitoring Based on Remotely Sensed Spectral Diversity—A Review. Remote Sens. 14, 5363. https://doi.org/10.3390/rs14215363

Katingan Mentaya Project, 2023. Katingan Mentaya Project [WWW Document]. URL https://katinganproject.com/ (accessed 5.26.23).

Kellner, J.R., Armston, J., Duncanson, L., 2023. Algorithm Theoretical Basis Document for GEDI Footprint Aboveground Biomass Density. Earth Space Sci. 10, e2022EA002516. https://doi.org/10.1029/2022EA002516

Khalefa, E., Smit, I.P.J., Nickless, A., Archibald, S., Comber, A., Balzter, H., 2013. Retrieval of Savanna Vegetation Canopy Height from ICESat-GLAS Spaceborne LiDAR With Terrain Correction. IEEE Geosci. Remote Sens. Lett. 10, 1439–1443. https://doi.org/10.1109/LGRS.2013.2259793

Kingma, D.P., Ba, J., 2014. Adam: A Method for Stochastic Optimization. https://doi.org/10.48550/ARXIV.1412.6980

Kulawardhana, R.W., Popescu, S.C., Feagin, R.A., 2014. Fusion of lidar and multispectral data to quantify salt marsh carbon stocks. Remote Sens. Environ. 154, 345–357. https://doi.org/10.1016/j.rse.2013.10.036

Lang, M., Binder, M., Richter, J., Schratz, P., Pfisterer, F., Coors, S., Au, Q., Casalicchio, G., Kotthoff, L., Bischl, B., 2019. mlr3: A modern object-oriented machine learning framework in R. J. Open Source Softw. 4, 1903. https://doi.org/10.21105/joss.01903

Lang, N., Jetz, W., Schindler, K., Wegner, J.D., 2022a. A high-resolution canopy height model of the Earth. https://doi.org/10.48550/arXiv.2204.08322

Lang, N., Kalischek, N., Armston, J., Schindler, K., Dubayah, R., Wegner, J.D., 2022b. Global canopy height regression and uncertainty estimation from GEDI LIDAR waveforms with deep ensembles. Remote Sens. Environ. 268, 112760. https://doi.org/10.1016/j.rse.2021.112760

Lang, N., Schindler, K., Wegner, J.D., 2019. Country-wide high-resolution vegetation height mapping with Sentinel-2. Remote Sens. Environ. 233, 111347. https://doi.org/10.1016/j.rse.2019.111347

Leuschner, C., Zach, A., Moser, G., Homeier, J., Graefe, S., Hertel, D., Wittich, B., Soethe, N., Iost, S., Röderstein, M., Horna, V., Wolf, K., 2013. The Carbon Balance of Tropical Mountain Forests Along an Altitudinal Transect, in: Bendix, J., Beck, E., Bräuning, A., Makeschin, F., Mosandl, R., Scheu, S., Wilcke, W. (Eds.), Ecosystem Services, Biodiversity and Environmental Change in a Tropical Mountain Ecosystem of South Ecuador, Ecological Studies. Springer Berlin Heidelberg, Berlin, Heidelberg, pp. 117–139. https://doi.org/10.1007/978-3-642-38137-9_10

Li, W., Niu, Z., Shang, R., Qin, Y., Wang, L., Chen, H., 2020. High-resolution mapping of forest canopy height using machine learning by coupling ICESat-2 LiDAR with Sentinel-1, Sentinel-2 and Landsat-8 data. Int. J. Appl. Earth Obs. Geoinformation 92, 102163. https://doi.org/10.1016/j.jag.2020.102163

Lim, K., Treitz, P., Wulder, M., St-Onge, B., Flood, M., 2003. LIDAR remote sensing of forest structure. Prog. Phys. Geogr. 27, 88–106. https://doi.org/10.1191/0309133303pp360ra

Lin, C., Labzovskii, L.D., Leung Mak, H.W., Fung, J.C.H., Lau, A.K.H., Kenea, S.T., Bilal, M., Vande Hey, J.D., Lu, X., Ma, J., 2020. Observation of PM2.5 using a combination of satellite remote sensing and low-cost sensor network in Siberian urban areas with limited reference monitoring. Atmos. Environ. 227, 117410. https://doi.org/10.1016/j.atmosenv.2020.117410

Liu, Y., Gong, W., Xing, Y., Hu, X., Gong, J., 2019. Estimation of the forest stand mean height and aboveground biomass in Northeast China using SAR Sentinel-1B, multispectral Sentinel-2A, and DEM imagery. ISPRS J. Photogramm. Remote Sens. 151, 277–289. https://doi.org/10.1016/j.isprsjprs.2019.03.016

Longo, M., Saatchi, S., Keller, M., Bowman, K., Ferraz, A., Moorcroft, P.R., Morton, D.C., Bonal, D., Brando, P., Burban, B., Derroire, G., dos-Santos, M.N., Meyer, V., Saleska, S., Trumbore, S., Vincent, G., 2020. Impacts of Degradation on Water, Energy, and Carbon Cycling of the Amazon Tropical Forests. J. Geophys. Res. Biogeosciences 125. https://doi.org/10.1029/2020JG005677

Louhaichi, M., Borman, M.M., Johnson, D.E., 2001. Spatially Located Platform and Aerial Photography for Documentation of Grazing Impacts on Wheat. Geocarto Int. 16, 65–70. https://doi.org/10.1080/10106040108542184
Mahoney, M.J., Johnson, L.K., Silge, J., Frick, H., Kuhn, M., Beier, C.M., 2023. Assessing the performance of spatial cross-validation approaches for models of spatially structured data. https://doi.org/10.48550/ARXIV.2303.07334
Main-Knorn, M., Cohen, W.B., Kennedy, R.E., Grodzki, W., Pflugmacher, D., Griffiths, P., Hostert, P., 2013. Monitoring coniferous forest biomass change using a Landsat trajectory-based approach. Remote Sens. Environ. 139, 277–290. https://doi.org/10.1016/j.rse.2013.08.010
Manning, P., van der Plas, F., Soliveres, S., Allan, E., Maestre, F.T., Mace, G., Whittingham, M.J., Fischer, M., 2018. Redefining ecosystem multifunctionality. Nat. Ecol. Evol. 2, 427–436. https://doi.org/10.1038/s41559-017-0461-7
McIntire, C.D., Cunliffe, A.M., Boschetti, F., Litvak, M.E., 2022. Allometric Relationships for Predicting Aboveground Biomass, Sapwood, and Leaf Area of Two-Needle Piñon Pine (Pinus edulis) Amid Open-Grown Conditions in Central New Mexico. For. Sci. fxac001. https://doi.org/10.1093/forsci/fxac001
Meyer, V., Saatchi, S., Clark, D.B., Keller, M., Vincent, G., Ferraz, A., Espírito-Santo, F., d'Oliveira, M.V.N., Kaki, D., Chave, J., 2018. Canopy area of large trees explains aboveground biomass variations across neotropical forest landscapes. Biogeosciences 15, 3377–3390. https://doi.org/10.5194/bg-15-3377-2018
Millennium Ecosystem Assessment, 2005. Ecosystems and Human Well-being: Synthesis.
Mills, M.B., Malhi, Y., Ewers, R.M., Kho, L.K., Teh, Y.A., Both, S., Burslem, D.F.R.P., Majalap, N., Nilus, R., Huaraca Huasco, W., Cruz, R., Pillco, M.M., Turner, E.C., Reynolds, G., Riutta, T., 2023. Tropical forests post-logging are a persistent net carbon source to the atmosphere. Proc. Natl. Acad. Sci. 120, e2214462120. https://doi.org/10.1073/pnas.2214462120
Mitchard, E.T.A., 2018. The tropical forest carbon cycle and climate change. Nature 559, 527–534. https://doi.org/10.1038/s41586-018-0300-2
Moran, P.A.P., 1950. Notes on Continuous Stochastic Phenomena. Biometrika 37, 17. https://doi.org/10.2307/2332142
Mulatu, K., Decuyper, M., Brede, B., Kooistra, L., Reiche, J., Mora, B., Herold, M., 2019. Linking Terrestrial LiDAR Scanner and Conventional Forest Structure Measurements with Multi-Modal Satellite Data. Forests 10, 291. https://doi.org/10.3390/f10030291
Naime, J., Mora, F., Sánchez-Martínez, M., Arreola, F., Balvanera, P., 2020. Economic valuation of ecosystem services from secondary tropical forests: trade-offs and implications for policy making. For. Ecol. Manag. 473, 118294. https://doi.org/10.1016/j.foreco.2020.118294
Nandy, S., Srinet, R., Padalia, H., 2021. Mapping Forest Height and Aboveground Biomass by Integrating ICESat-2, Sentinel-1 and Sentinel-2 Data Using Random Forest Algorithm in Northwest Himalayan Foothills of India. Geophys. Res. Lett. 48, e2021GL093799. https://doi.org/10.1029/2021GL093799
NICFI, 2020. Norway's International Climate and Forest Initiative - About us [WWW Document]. NICFI. URL https://www.nicfi.no/about-us/ (accessed 7.24.23).
Ota, T., Ahmed, O., Franklin, S., Wulder, M., Kajisa, T., Mizoue, N., Yoshida, S., Takao, G., Hirata, Y., Furuya, N., Sano, T., Heng, S., Vuthy, M., 2014. Estimation of Airborne Lidar-Derived Tropical Forest Canopy Height Using Landsat Time Series in Cambodia. Remote Sens. 6, 10750–10772. https://doi.org/10.3390/rs61110750
Pan, Y., Birdsey, R.A., Fang, J., Houghton, R., Kauppi, P.E., Kurz, W.A., Phillips, O.L., Shvidenko, A., Lewis, S.L., Canadell, J.G., Ciais, P., Jackson, R.B., Pacala, S.W., McGuire, A.D., Piao, S., Rautiainen, A., Sitch, S., Hayes, D., 2011. A Large and Persistent Carbon Sink in the World's Forests. Science 333, 988–993. https://doi.org/10.1126/science.1201609
Permian Global, 2023a. Permian Global [WWW Document]. URL https://permianglobal.com/ (accessed 5.17.23).
Permian Global, 2023b. The Katingan Mentaya Project protects Indonesian peatland forests | Katingan Mentaya Project [WWW Document]. Permian Glob. URL https://permianglobal.com/our-work/katingan-mentaya-project/ (accessed 5.26.23).
Pinty, B., Verstraete, M.M., 1992. GEMI: a non-linear index to monitor global vegetation from satellites. Vegetatio 101, 15–20. https://doi.org/10.1007/BF00031911

Planet Labs, 2023a. PlanetScope [WWW Document]. URL https://developers.planet.com/docs/data/planetscope/ (accessed 7.20.23).
Planet Labs, 2023b. NICFI Program - Satellite Imagery and Monitoring [WWW Document]. Planet. URL https://www.planet.com/nicfi/ (accessed 7.24.23).
Planet Labs, 2023c. UDM 2 [WWW Document]. Planet Dev. URL https://developers.planet.com/docs/data/udm-2/ (accessed 7.27.23).
Pourshamsi, M., Xia, J., Yokoya, N., Garcia, M., Lavalle, M., Pottier, E., Balzter, H., 2021. Tropical forest canopy height estimation from combined polarimetric SAR and LiDAR using machine-learning. ISPRS J. Photogramm. Remote Sens. 172, 79–94. https://doi.org/10.1016/j.isprsjprs.2020.11.008
PT Map Tiga Internasional, 2022. 2022 Topographic LiDAR Survey Project Report for PT Rimba Makmur Utama.
R Core Team, 2022. R: A language and environment for statistical computing.
Reid, W.V., 1998. Biodiversity hotspots. Trends Ecol. Evol. 13, 275–280. https://doi.org/10.1016/S0169-5347(98)01363-9
Rikimaru, A., Roy, P., Miyatake, S., 2002. Tropical forest cover density mapping. Trop. Ecol. 43, 39–47.
Rischbeck, P., Elsayed, S., Mistele, B., Barmeier, G., Heil, K., Schmidhalter, U., 2016. Data fusion of spectral, thermal and canopy height parameters for improved yield prediction of drought stressed spring barley. Eur. J. Agron. 78, 44–59. https://doi.org/10.1016/j.eja.2016.04.013
Rösch, M., Sonnenschein, R., Buchelt, S., Ullmann, T., 2022. Comparing PlanetScope and Sentinel-2 Imagery for Mapping Mountain Pines in the Sarntal Alps, Italy. Remote Sens. 14, 3190. https://doi.org/10.3390/rs14133190
Roujean, J.-L., Breon, F.-M., 1995. Estimating PAR absorbed by vegetation from bidirectional reflectance measurements. Remote Sens. Environ. 51, 375–384. https://doi.org/10.1016/0034-4257(94)00114-3
Rouse, J.W., Jr., Haas, R.H., Schell, J.A., Deering, D.W., 1974. Monitoring Vegetation Systems in the Great Plains with Erts. NASA Spec. Publ. 351, 309.
Sandonís Pozo, L., Plata Moreno, J.M., Llorens Calveras, J., Escolà i Agustí, A., Pascual Roca, M., Martínez Casasnovas, J.A., 2022. PlanetScope Vegetation Indices to Estimate UAV and LiDAR-derived Canopy Parameters in a Super-Intensive Almond Orchard.
Schneider, L., Richter, J., Becker, M., Lang, M., Bischl, B., Pfisterer, F., Binder, M., Fischer, S., 2023. Flexible Bayesian Optimization.
Sentinel-Hub, 2023a. PlanetScope [WWW Document]. PlanetScope. URL https://docs.sentinel-hub.com/api/latest/data/planet/planet-scope/ (accessed 7.20.23).
Sentinel-Hub, 2023b. Sentinel-2 Bands [WWW Document]. Sentin. Hub Cust. Scr. URL https://custom-scripts.sentinel-hub.com/custom-scripts/sentinel-2/bands/ (accessed 8.16.23).
Shah, S.A.A., Manzoor, M.A., Bais, A., 2020. Canopy Height Estimation at Landsat Resolution Using Convolutional Neural Networks. Mach. Learn. Knowl. Extr. 2, 23–36. https://doi.org/10.3390/make2010003
Sharma, R., Rimal, B., Baral, H., Nehren, U., Paudyal, K., Sharma, S., Rijal, S., Ranpal, S., Acharya, R.P., Alenazy, A.A., Kandel, P., 2019. Impact of Land Cover Change on Ecosystem Services in a Tropical Forested Landscape. Resources 8, 18. https://doi.org/10.3390/resources8010018
Sheridan, R., Popescu, S., Gatziolis, D., Morgan, C., Ku, N.-W., 2014. Modeling Forest Aboveground Biomass and Volume Using Airborne LiDAR Metrics and Forest Inventory and Analysis Data in the Pacific Northwest. Remote Sens. 7, 229–255. https://doi.org/10.3390/rs70100229
Shimizu, K., Ota, T., Mizoue, N., Saito, H., 2020. Comparison of Multi-Temporal PlanetScope Data with Landsat 8 and Sentinel-2 Data for Estimating Airborne LiDAR Derived Canopy Height in Temperate Forests. Remote Sens. 12, 1876. https://doi.org/10.3390/rs12111876
Simoes, R., Souza, F., Zaglia, M., Ribeiro Queiroz, G., Santos, R., Ferreira, K., n.d. Rstac: An R Package to Access Spatiotemporal Asset Catalog Satellite Imagery.
Simon, R., 2007. Resampling Strategies for Model Assessment and Selection, in: Dubitzky, W., Granzow, M., Berrar, D. (Eds.), Fundamentals of Data Mining in Genomics and Proteomics. Springer US, Boston, MA, pp. 173–186. https://doi.org/10.1007/978-0-387-47509-7_8
Staben, G., Lucieer, A., Scarth, P., 2018. Modelling LiDAR derived tree canopy height from Landsat TM, ETM+ and OLI satellite imagery—A machine learning approach. Int. J. Appl. Earth Obs. Geoinformation 73, 666–681. https://doi.org/10.1016/j.jag.2018.08.013

STAC, 2023. STAC: SpatioTemporal Asset Catalogs [WWW Document]. URL https://stacspec.org/en/ (accessed 7.27.23).

Strassburg, B.B.N., Iribarrem, A., Beyer, H.L., Cordeiro, C.L., Crouzeilles, R., Jakovac, C.C., Braga Junqueira, A., Lacerda, E., Latawiec, A.E., Balmford, A., Brooks, T.M., Butchart, S.H.M., Chazdon, R.L., Erb, K.-H., Brancalion, P., Buchanan, G., Cooper, D., Díaz, S., Donald, P.F., Kapos, V., Leclère, D., Miles, L., Obersteiner, M., Plutzar, C., de M. Scaramuzza, C.A., Scarano, F.R., Visconti, P., 2020. Global priority areas for ecosystem restoration. Nature 586, 724–729. https://doi.org/10.1038/s41586-020-2784-9

Takagi, K., Yone, Y., Takahashi, H., Sakai, R., Hojyo, H., Kamiura, T., Nomura, M., Liang, N., Fukazawa, T., Miya, H., Yoshida, T., Sasa, K., Fujinuma, Y., Murayama, T., Oguma, H., 2015. Forest biomass and volume estimation using airborne LiDAR in a cool-temperate forest of northern Hokkaido, Japan. Ecol. Inform. 26, 54–60. https://doi.org/10.1016/j.ecoinf.2015.01.005

Torres de Almeida, C., Gerente, J., Rodrigo dos Prazeres Campos, J., Caruso Gomes Junior, F., Providelo, L.A., Marchiori, G., Chen, X., 2022. Canopy Height Mapping by Sentinel 1 and 2 Satellite Images, Airborne LiDAR Data, and Machine Learning. Remote Sens. 14, 4112. https://doi.org/10.3390/rs14164112

Valluvan, A.B., Raj, R., Pingale, R., Jagarlapudi, A., 2023. Canopy height estimation using drone-based RGB images. Smart Agric. Technol. 4, 100145. https://doi.org/10.1016/j.atech.2022.100145

Veloz, S.D., 2009. Spatially autocorrelated sampling falsely inflates measures of accuracy for presence-only niche models. J. Biogeogr. 36, 2290–2299. https://doi.org/10.1111/j.1365-2699.2009.02174.x

Vincini, M., Frazzi, E., 2011. Comparing narrow and broad-band vegetation indices to estimate leaf chlorophyll content in planophile crop canopies. Precis. Agric. 12, 334–344. https://doi.org/10.1007/s11119-010-9204-3

Wang, C., Glenn, N., 2008. A linear regression method for tree canopy height estimation using airborne lidar data. Can. J. Remote Sens. 34. https://doi.org/10.5589/m08-043

Wang, F., Huang, J., Tang, Y., Wang, X., 2007. New Vegetation Index and Its Application in Estimating Leaf Area Index of Rice. Rice Sci. 14, 195–203. https://doi.org/10.1016/S1672-6308(07)60027-4

Wang, H., Seaborn, T., Wang, Z., Caudill, C., Link, T., 2021. Modeling tree canopy height using machine learning over mixed vegetation landscapes. Int. J. Appl. Earth Obs. Geoinformation 101, 102353. https://doi.org/10.1016/j.jag.2021.102353

Wilkes, P., Jones, S., Suarez, L., Mellor, A., Woodgate, W., Soto-Berelov, M., Haywood, A., Skidmore, A., 2015. Mapping Forest Canopy Height Across Large Areas by Upscaling ALS Estimates with Freely Available Satellite Data. Remote Sens. 7, 12563–12587. https://doi.org/10.3390/rs70912563

Wood, E.M., Pidgeon, A.M., Radeloff, V.C., Keuler, N.S., 2012. Image texture as a remotely sensed measure of vegetation structure. Remote Sens. Environ. 121, 516–526. https://doi.org/10.1016/j.rse.2012.01.003

Wright, M.N., Ziegler, A., 2015. ranger: A Fast Implementation of Random Forests for High Dimensional Data in C++ and R. https://doi.org/10.48550/ARXIV.1508.04409

Xi, Z., Xu, H., Xing, Y., Gong, W., Chen, G., Yang, S., 2022. Forest Canopy Height Mapping by Synergizing ICESat-2, Sentinel-1, Sentinel-2 and Topographic Information Based on Machine Learning Methods. Remote Sens. 14, 364. https://doi.org/10.3390/rs14020364

Zhang, L., Shao, Z., Liu, J., Cheng, Q., 2019. Deep Learning Based Retrieval of Forest Aboveground Biomass from Combined LiDAR and Landsat 8 Data. Remote Sens. 11, 1459. https://doi.org/10.3390/rs11121459

Zhang, N., Chen, M., Yang, F., Yang, C., Yang, P., Gao, Y., Shang, Y., Peng, D., 2022. Forest Height Mapping Using Feature Selection and Machine Learning by Integrating Multi-Source Satellite Data in Baoding City, North China. Remote Sens. 14, 4434. https://doi.org/10.3390/rs14184434